Journal of Applied Analysis and Computation
Volume 16, Number 2, April 2026, 665–704
Website:http://www.jaac-online.com
DOI:10.11948/20250047

GLOBAL DYNAMICS OF TWO-SPECIES AMENSALISM SYSTEM WITH SATURATED FEAR AND ALLEE EFFECTS

Yuting Huang[1], Fengde Chen[1,†], Zhong Li[1] and Lijuan Chen[1]

Abstract This paper proposes and investigates a two-species amensalism system incorporating a Holling-II functional response, which integrates both the saturated fear effect and the Allee effect on the first species. We first establish sufficient conditions for the existence and stability of equilibrium points, analyzing saddle-node, transcritical and pitchfork bifurcations while conducting comprehensive global dynamics analysis. Subsequently, stochastic perturbations are introduced to construct a random system, where we observe noise-induced state transitions and estimate the critical noise threshold for such transitions. Finally, numerical simulations are performed to validate the feasibility of the theoretical results. The study shows that excessively high fear does not necessarily lead to the extinction of the first species. Specifically, when the saturation fear parameter exceeds a certain threshold, the first species persists even under extreme fear conditions; however, when below this threshold, high fear levels still lead to extinction, though weak Allee effects significantly slow this process.

Keywords Amensalism model, saturated fear effect, Allee effect, bifurcation, global dynamics.

MSC(2010) 34C23, 34D20, 34H10, 92D25.

1. Introduction

Interactions among species in nature are complex and vital to ecosystem structure and dynamics. Amensalism, an asymmetric interaction where one species negatively affects another without being impacted itself, is widespread in ecosystems. However, the role of the saturated fear effect in such systems remains underexplored. This interaction is widespread among plants, microorganisms, and animal groups. For example, some plants release allelopathic chemicals that inhibit the growth of neighboring plants without affecting themselves [23]. Another example involves the interaction between bacteria and fungi, where certain fungi secrete antibiotics that suppress bacterial growth without impacting their own growth [13].

Over the past decade, significant advances have been made in the study of amensalism relationships and population dynamics models. Sun [28] first introduced the following population amensalism model:

$$\begin{cases} \dfrac{dx}{dt} = r_1 x\left(\dfrac{k_1 - x - cy}{k_1}\right), \\ \dfrac{dy}{dt} = r_2 y\left(\dfrac{k_2 - y}{k_2}\right), \end{cases} \tag{1.1}$$

†The corresponding author.
[1]School of Mathematics and Statistics, Fuzhou University, Fuzhou 350116, China
Email: 1104943637@qq.com(Y. Huang), fdchen@fzu.edu.cn(F. Chen), lizhong04108@163.com(Z. Li), chenlijuan@fzu.edu.cn(L. Chen)

where $x(t)$ and $y(t)$ represent the population densities of the first and second species at time t, respectively; r_i represent the intrinsic growth rates of the two species, while k_i indicate their environmental carrying capacities. The coefficient c shows how one member of species y affects species x.

In the following years, many scholars proposed various models on amensalism and analyzed their dynamical behaviors [2,4,5,10,16,17,20,21,27,32–34,38,40,41,44–46]. Additionally, scholars have suggested that nonlinear functions may better capture the effect of the second group on the first group than linear functions [10,18,21,22,33,46]. Specifically, Luo [21] introduced an amensalism model incorporating a Holling-II functional response and the Allee effect for the first species, along with a nonlinear birth rate for the second species. The model is expressed as:

$$\begin{cases} \dfrac{dx}{dt} = x\left(a_1 - b_1 x - \dfrac{cy}{m+nx}\right)\left(\dfrac{x}{\gamma + x}\right), \\ \dfrac{dy}{dt} = y\left(\dfrac{\alpha}{1+\beta y} - b_2 y\right), \end{cases} \tag{1.2}$$

where a_1 and $\frac{\alpha}{1+\beta y}$ denote the intrinsic growth rates of the two species, b_i represent their intraspecific competition coefficients, m and n represent the half-saturation constant and scaling coefficient respectively, while γ quantifies the intensity of the Allee effect. The author analyzed the stability of the equilibria, bifurcation scenarios and the global structure of the system. The Allee effect was observed to extend the time the system takes to achieve the steady-state rather than affect the final stable steady-state solution of the system.

Recently, the impact of the fear effect on species interactions has attracted significant scholarly attention. The fear effect refers to behavioral and physiological changes in prey species caused by the mere presence of predators, even without actual predation. These changes impact their survival and reproduction. However, this phenomenon is not limited to predator-prey relationships but is also observed in amensalism interactions. In the experiment conducted by Xi [37], four experimental groups were set up: a plant community with only grasshoppers, a plant community with only caterpillars, a plant community with both grasshoppers and caterpillars, and a control group without either. The researchers compared the oviposition rates and larval survival rates of caterpillars across these groups. The results showed that the oviposition rates and larval survival rates of caterpillars were significantly lower in plant communities with both grasshoppers and caterpillars than in communities with only caterpillars. This experiment demonstrated that grasshopper-induced fear reduced the reproductive rate of caterpillars, resulting in a significant decline in offspring numbers. Therefore, introducing the fear effect into the study of amensalism interactions is of great significance. Based on this finding, Chong [7] proposed an amensalism model, assuming that the second population induces fear in the first population, thereby reducing its birth rate and increasing its death rate. The model is expressed as:

$$\begin{cases} \dfrac{dx_1}{dt} = x_1\left(\dfrac{e_1}{1+k_1 x_2} - (1+k_2 x_2)e_2 - b_1 x_1 - c x_2\right), \\ \dfrac{dx_2}{dt} = x_2\left(a_2 - b_2 x_2\right), \end{cases} \tag{1.3}$$

where e_i represent the birth rate and mortality rate of the first species, $\frac{1}{1+k_1 x_2}$ and $1+k_2 x_2$ are the fear effect, and k_i denote the fear level. Their study shows that as the intensity of the fear effect increases, the population density of the first species decreases, and when the fear effect

reaches a critical level, it may lead to extinction. Subsequently, Zhu [46] proposed an amensalism model that incorporates the fear effect on the first species along with a Beddington-DeAngelis functional response. The model is expressed as:

$$\begin{cases} \dfrac{dx}{dt} = x\left(\dfrac{a_1}{1+k_1y} - d_1 - b_1x - \dfrac{cxy}{1+mx+ny}\right), \\ \dfrac{dy}{dt} = y\Big(a_2 - b_2y\Big), \end{cases} \tag{1.4}$$

where the term $\frac{cxy}{1+mx+ny}$ represents the Beddington-DeAngelis functional response, and m and n correspond to the handling time coefficient of the first species and the interference coefficient of the second species, respectively. Their study revealed that under certain parameter conditions, when the intensity of the fear effect is below a specific threshold, increasing the fear effect only reduces the population density of the first species without influencing its persistence or extinction. However, when the fear effect surpasses this threshold, further increases in fear will accelerate the extinction of the first species.

In practice, fear alone does not necessarily result in the extinction of the first species. Akimoto [1] discovered through experiments conducted on the Hokkaido University campus in Japan that interspecific interactions within the genus Tetraneura on elm trees exhibited an amensalistic relationship. Specifically, coexistence of galls (tumor-like structures formed due to aphid-induced abnormal plant tissue growth) of the same or different species on a single leaf had no impact on the reproductive capacity of other aphid species, but negatively affected sp. O (a species not yet fully classified or formally named). However, the average reproductive capacity of the negatively impacted species (sp. O) exceeded that of other species. For sp. O, the amensalistic effect contributed only a small fraction to the variation in reproductive capacity. Experimental results showed that 45.7% of the elm trees hosted galls from multiple species (including those of sp. O), suggesting that under the influence of amensalism, populations could still coexist and the effects were insufficient to drive sp. O to extinction. Furthermore, according to experimental data from Xi [37], the survival rate of mixed larvae was significantly lower than that of isolated larvae, but the decline in survival rate was marginal and did not result in the extinction of caterpillar larvae in the mixed experiments.

Building on these experimental findings, we refer to a new fear function proposed by Dong [9]: $f(k,\eta,y) = \eta + \frac{1-\eta}{1+ky}$ to better capture the fear effect. This function demonstrates that as the fear level k increases, the fear function $f(k,\eta,y)$ diminishes. In other words, greater fear leads to higher fear costs, which in turn decreases the prey's reproduction rate. Nevertheless, this decrease does not occur indefinitely. Ultimately, the fear function $f(k,\eta,y)$ will approach a saturation value η. From an ecological perspective, this assumption is more reasonable.

Inspired by the research of Chong [7] and Dong [9], and recognizing that no amensalism model incorporating a saturated fear effect has yet been proposed or studied, we were motivated to propose the following model:

$$\begin{cases} \dfrac{dx_1}{d\tau} = x_1\left(a_1(\eta_1 + \dfrac{1-\eta_1}{1+k_1x_2}) - d_1 - b_1x_1 - \dfrac{c_1x_2}{m+nx_1}\right), \\ \dfrac{dx_2}{d\tau} = x_2(a_2 - b_2x_2), \end{cases} \tag{1.5}$$

where $x_1(\tau)$ and $x_2(\tau)$ denote the first and second species densities at time τ, respectively. For system (1.5), we make the following assumptions:

(1) The second species follows Logistic growth;

(2) where a_1, d_1 and b_1 represent the birth rate, mortality rate and intraspecific competition mortality rate of the first species. If the birth rate is lower than the mortality rate, the first species will risk extinction. This research assumes $a_1 > d_1$ to study the two species' connection;

(3) the damage inflicted by the second species on the first species adheres to the Holling-II functional response, expressed as $\frac{c_1 x_2}{m+nx_1}$;

(4) to account for the fear factor, we use the saturated fear function $f(k_1, \eta_1, x_2)=\eta_1 + \frac{1-\eta_1}{1+k_1 x_2}$, where the fear parameter is $k_1 \geq 0$ and the saturated fear parameter is $\eta_1 \in [0, 1]$. And for the saturated fear function $f(k_1, \eta_1, x_2)$, we easily obtain that $f(k_1, \eta_1, x_2) \to \eta_1$ as $k_1 \to \infty$ or $x_2 \to \infty$.

To minimize the parameters of system (1.5), the following dimensionless quantities are used in system (1.5),

$$\begin{aligned} &\frac{n}{m}x_1 = x, x_2 = y,\ a_2\tau = t,\ \frac{a_1}{a_2} = a,\ k_1 = k,\\ &\eta_1 = \eta,\ \frac{d_1}{a_2} = d,\ \frac{b_1 m}{a_2 n} = b,\ \frac{c_1}{a_2 m} = c,\ \frac{b_2}{a_2} = e, \end{aligned} \tag{1.6}$$

then system (1.5) becomes the following system:

$$\begin{cases} \dfrac{dx}{dt} = x\left(a(\eta + \dfrac{1-\eta}{1+ky}) - d - bx - \dfrac{cy}{1+x}\right), \\ \dfrac{dy}{dt} = y(1-ey), \end{cases} \tag{1.7}$$

where a, b, c, d, k, η and e are all positive constants, and $k \geq 0$, $0 \leq \eta \leq 1$. For the saturated fear parameter η, it is used to characterize the upper limit of the fear effect. When η is relatively small, the density of the second species increases, the fear effect can still significantly suppress the survival of the first species. As η increases, the first species to persist even in high-fear environments. This study demonstrates that when η is small, the first species may struggle to survive and could even face extinction. However, when η exceeds a certain critical threshold, the system may shift from an extinction state to a bistable state, or maybe attain stable coexistence.

Allee effect is a key population dynamics phenomenon that may impact species interactions. This shows that population size increases fitness. In ecological models, the Allee effect shows that low densities limit population development, which might lead to extinction if the population falls below a crucial threshold. Allee effect adds complexity to amensalism models. Scholars have lately begun studying this impact [11, 14, 19, 21, 26, 32, 33, 39, 43]. For example, in their study on the Allee effect in the first species, Luo [21] discoverd that system having the Allee effect requires longer to obtain a stable steady-state solution. Now, an interesting issue is proposed: If the first species exhibits both the saturated fear effect and the Allee effect, what dynamic behavior would the system exhibit? A two-species Holling-II amensalism system incorporating the saturated fear effect and weak Allee effect can be formulated as follows:

$$\begin{cases} \dfrac{dx_1}{d\tau} = x_1\left(a_1(\eta_1 + \dfrac{1-\eta_1}{1+k_1 x_2}) - d_1 - b_1 x_1 - \dfrac{c_1 x_2}{m+nx_1}\right) \\ \qquad\qquad \times\left(\dfrac{x_1}{x_1+u}\right), \\ \dfrac{dx_2}{d\tau} = x_2(a_2 - b_2 x_2). \end{cases} \tag{1.8}$$

Here, we define $F(x_1) = \frac{x_1}{x_1+u}$ to represent the Allee effect on the first species, where u is a positive constant that determines the intensity of the Allee effect.

In our model, we adopted the weak Allee effect rather than the strong Allee effect based on the following considerations: First, the weak Allee effect manifests as a reduction in population growth rate with decreasing density, while the rate remains positive throughout. In contrast, the strong Allee effect involves a critical threshold below which the growth rate becomes negative. The weak Allee effect better aligns with our study, where the presence of a saturated fear effect ensures that the population growth rate remains positive. As demonstrated in Schreiber [26], most species exhibiting the Allee effect display the "weak" form. From a modeling perspective, the weak Allee effect function $F(x_1) = \frac{x_1}{x_1+u}$ maintains continuity and differentiability, avoiding potential numerical instability issues associated with the strong Allee effect. From an ecological conservation standpoint, the weak Allee effect better reflects the "early warning" concept in conservation biology. It captures the state of population decline before reaching an irreversible threshold, making it more biologically meaningful for assessing population dynamics under stress.

To minimize the parameters of system (1.8), we similarly apply the transformation from (1.6). System (1.8) can be simplified to system (1.9).

$$\begin{cases} \dfrac{dx}{dt} = x\left(a(\eta + \dfrac{1-\eta}{1+ky}) - d - bx - \dfrac{cy}{1+x}\right)\left(\dfrac{x}{x+u}\right), \\ \dfrac{dy}{dt} = y(1-ey). \end{cases} \tag{1.9}$$

This paper will focus on the global dynamics of system (1.7) and system (1.9). In the second part of this paper, we first present adequate requirements to guarantee the existence and stability of all possible equilibria of system (1.7). Additionally, we analyze key conditions that guarantee the occurrence of bifurcations in system (1.7). Subsequently, the global structure of system (1.7) in the first quadrant is analyzed, and the corresponding global phase diagram is provided. The third section employs numerical simulations to investigate the effects of environmental noise under bistable conditions, where we quantitatively estimate the critical noise threshold triggering state transitions through the construction of confidence ellipses. In the fourth part, we similarly examine the equilibrium points, stability, and bifurcations of system (1.9). In the fifth part, numerical simulations of the dynamics of both system (1.7) and system (1.9) are performed to validate the theoretical results, revealing specific dynamic behaviors. Finally, we present the conclusion in the sixth part.

This study is the first to introduce the saturated fear effect into an amensalism system. The main aim of this study is to examine the influence of the saturated fear effect and the Allee effect on the system's dynamic behavior. Specifically, when the saturated fear parameter exceeds a certain threshold, even extremely high fear levels will not result in the extinction of the first species. Under these conditions, the system exhibits bistability. To better align this coexistence phenomenon with ecological reality, we incorporated environmental noise into a stochastic system framework and employed stochastic sensitivity function techniques to quantitatively estimate the critical noise threshold governing the transition from stable coexistence to extinction of the first species. However, when the saturated fear parameter falls below this threshold, excessively high fear levels can still result in the extinction of the first species, but the presence of the weak Allee effect significantly slows down the extinction process. These findings not only fill a crucial gap in understanding saturated fear effects in amensalism systems, but also enhance our ability to predict population dynamics in natural systems subject to stochastic disturbances.

2. Global dynamics of system (1.7)

2.1. Existence of equilibria

Regarding the discussion on the existence of equilibria of system (1.7), setting $\frac{dx}{dt} = \frac{dy}{dt} = 0$ in the system (1.7), we obtain

$$\begin{cases} x\left(a(\eta + \dfrac{1-\eta}{1+ky}) - d - bx - \dfrac{cy}{1+x}\right) = 0, \\ y(1-ey) = 0. \end{cases} \tag{2.1}$$

It is clear from (2.1) that system (1.7) has three boundary equilibria: $E_0(0,0)$, $E_1(\frac{a-d}{b}, 0)$ and $E_2(0, \frac{1}{e})$. For the positive equilibria $E_i^*(x_i^*, y^*)$, it is clear that $y^* = \frac{1}{e}$.

We denote

$$F(x) = Ax^2 + Bx + C, \tag{2.2}$$

where

$$\begin{aligned} A &= be^2 + bke, \\ B &= -(-b + a - d)e^2 - k(a\eta - b - d)e, \\ C &= -(a-d)e^2 - ((a\eta - d)k - c)e + ck. \end{aligned}$$

The discriminant of $F(x)$ is given by

$$\begin{aligned} \Delta &= B^2 - 4AC \\ &= -4\left(be^2 + bke\right)\left(-\left(a-d\right)e^2 - \left(\left(a\eta - d\right)k - c\right)e + ck\right) \\ &\quad + \left(-\left(-b + a - d\right)e^2 - k\left(a\eta - b - d\right)e\right)^2. \end{aligned}$$

Obviously, if

$$0 < c < \frac{e(a\eta k + be + bk + ea - de - dk)^2}{4b(k+e)^2} \triangleq c^*, \tag{2.3}$$

then $F(x)$ has two roots

$$x_1^* = \frac{-B + \sqrt{\Delta}}{2A},\ x_2^* = \frac{-B - \sqrt{\Delta}}{2A},$$

and if $c = c^*$, $F(x)$ has a unique root

$$x_3^* = \frac{-B}{2A}.$$

Let $\eta = \frac{be+bk+de+dk-ea}{ka} \triangleq \eta^*$ and $b + d < a < \frac{(k+e)(b+d)}{e}$, we have $B = 0$. When $(-B)^2 = \Delta$, we can calculate that

$$c = \frac{e(a\eta k + ea - de - dk)}{k+e} \triangleq c^{**} > 0, \text{ if } \eta > \frac{de + dk - ea}{ka} \triangleq \eta^{**},\ d < a < \frac{d(k+e)}{e}. \tag{2.4}$$

Hence, it can be concluded that

(H_{1a}) If $\eta > \eta^*$ and $b + d < a < \frac{(k+e)(b+d)}{e}$, $-B > 0$.

(H_{1b}) If $\eta < \eta^*$ and $b + d < a < \frac{(k+e)(b+d)}{e}$, $-B < 0$.

(H_{2a}) If $c < c^{**}$, $\eta > \eta^{**}$ and $d < a < \frac{d(k+e)}{e}$, $(-B)^2 < \Delta$.

(H_{2b}) If $c > c^{**}$, $\eta > \eta^{**}$ and $d < a < \frac{d(k+e)}{e}$, $(-B)^2 > \Delta$.

We can simply confirm $c^{**} \le c^*$, $\eta^{**} < \eta^*$, and $c^{**} = c^*$ if and only if $B = 0$.

For conditions (2.3), (2.4), (H_{1a}),(H_{1b}),(H_{2a}) and (H_{2b}), we can draw the conclusion that:

(1) When $0 < c < c^{**}$, $\eta > \eta^{**}$ and $d < a < \frac{d(k+e)}{e}$, $x_1^* > 0$ and $x_2^* < 0$.

(2) When $c = c^{**}$,

(a) $x_1^* = 0$, $x_2^* < 0$ if $\eta^{**} < \eta < \eta^*$, $b + d < a < \frac{d(k+e)}{e}$ and $k > \frac{eb}{d}$;

(b) $x_1^* = x_2^* = 0$ if $\eta = \eta^*$, $b + d < a < \frac{d(k+e)}{e}$ and $k > \frac{eb}{d}$;

(c) $x_1^* > 0$, $x_2^* = 0$ if $\eta > \eta^*$, $b + d < a < \frac{d(k+e)}{e}$ and $k > \frac{eb}{d}$.

(3) When $c^{**} < c < c^*$,

(a) $x_1^* < 0$, $x_2^* < 0$ if $\eta^{**} < \eta < \eta^*$, $b + d < a < \frac{d(k+e)}{e}$ and $k > \frac{eb}{d}$;

(b) $x_1^* > 0$, $x_2^* > 0$ if $\eta > \eta^*$, $b + d < a < \frac{d(k+e)}{e}$ and $k > \frac{eb}{d}$.

(4) When $c = c^*$ (i.e., $\Delta = 0$), if $\eta > \eta^*$ and $b + d < a < \frac{(d+b)(k+e)}{e}$, $x_3^* > 0$.

(5) When $c > c^*$ (i.e., $\Delta < 0$), then $F(x)$ has no root.

Remark 2.1. For the purpose of categorization in subsequent discussions, it is assumed throughout the paper that wherever c^{**} and η^* appear, we default to $c^{**} > 0$ (i.e., $\eta > \eta^{**}$ and $d < a < \frac{d(k+e)}{e}$) and $\eta^* > 0$ (i.e., $b + d < a < \frac{(k+e)(b+d)}{e}$). In addition, when discussing the case where both c^{**} and η^* are greater than 0, we default that $d + b < a < \frac{d(k+e)}{e}$ if $k > \frac{eb}{d}$.

The analysis above yields the following theorem.

Theorem 2.1. *System (1.7) exhibits three boundary equilibria: $E_0(0,0)$ (both species extinct), $E_1(\frac{a-d}{b}, 0)$ (first species survives, second extinct) and $E_2(0, \frac{1}{e})$ (first species extinct, second survives). The following outcomes indicate positive equilibrium (coexistence of the two species):*
(1) For $0 < c < c^{**}$, then system (1.7) possesses one positive equilibrium $E_1^*(x_1^*, y^*)$.
(2) For $c = c^{**}$, then system (1.7) possesses one positive equilibrium $E_1^*(x_1^*, y^*)$ if $\eta > \eta^*$, and lacks positive equilibrium if $\eta^{**} < \eta \le \eta^*$.
(3) For $c^{**} < c < c^*$, then system (1.7) possesses two positive equilibria $E_1^*(x_1^*, y^*)$ and $E_2^*(x_2^*, y^*)$ if $\eta > \eta^*$, and lacks positive equilibrium if $\eta^{**} < \eta < \eta^*$.
(4) For $c = c^*$, then system (1.7) possesses one unique positive equilibrium $E_3^*(x_3^*, y^*)$ if $\eta > \eta^*$, and lacks positive equilibrium if $\eta^{**} < \eta < \eta^*$.
(5) For $c > c^*$, then system (1.7) lacks positive equilibrium.

Remark 2.2. From Theorem 2.1, it can be concluded that the core of the problem lies in the values of the parameters c, k and η. Specifically, c denotes the influence of an individual from the second species on the first species, k is the fear level, and η is the saturated fear parameter. In the subsequent analysis, we will discuss the effects of c, k and η on coexistence stability. The parameters c and η can serve both as global stability parameters and as bifurcation parameters in subsequent bifurcation analysis.

2.2. Stability of equilibria

Theorem 2.2. *For the boundary equilibria $E_0(0,0)$, $E_1(\frac{a-d}{b}, 0)$ and $E_2(0, \frac{1}{e})$ of system (1.7),*
(1) E_0 is an unstable node (Figure 1(a)).
(2) E_1 is a saddle (Figure 1(a)).
(3) For E_2,

(a) if $0 < c < c^{**}$, then E_2 is a saddle (Figure 1(a));

(b) if $c > c^{**}$, then E_2 is a stable node (Figure 1(b));

(c) if $c = c^{**}$, E_2 is an attracting saddle-node for $\eta \neq \eta^*$ and a degenerate stable node for $\eta = \eta^*$ (Figure 1(c)-1(d)).

Proof. The Jacobian matrix of system (1.7) is

$$J(E) = \begin{pmatrix} \Lambda_1 & \Lambda_2 \\ 0 & -2ey+1 \end{pmatrix}, \tag{2.5}$$

where

$$\Lambda_1 = a(\eta + \frac{1-\eta}{1+ky}) - d - bx - \frac{cy}{1+x} + x\Big(-b + \frac{cy}{(1+x)^2}\Big),$$
$$\Lambda_2 = x\Big(-\frac{a(1-\eta)k}{(ky+1)^2} - \frac{c}{1+x}\Big).$$

The Jacobian matrix at $E_0(0,0)$ and $E_1(\frac{a-d}{b},0)$ are

$$J(E_0) = \begin{pmatrix} a-d & 0 \\ 0 & 1 \end{pmatrix}, \tag{2.6}$$

and

$$J(E_1) = \begin{pmatrix} -a+d & -\dfrac{(a-d)\left(k\left(-1+\eta\right)a^2 + k\left(-1+\eta\right)(b-d)\,a - cb\right)}{b\,(b+a-d)} \\ 0 & 1 \end{pmatrix}, \tag{2.7}$$

respectively. Obviously, E_0 is an unstable node and E_1 is a saddle.

The Jacobian matrix at $E_2(0,\frac{1}{e})$ is

$$J(E_2) = \begin{pmatrix} \dfrac{(a-d)\,e^2 + ((a\eta-d)\,k-c)\,e - ck}{(k+e)e} & 0 \\ 0 & -1 \end{pmatrix}, \tag{2.8}$$

the two eigenvalues of $J(E_2)$ are expressed as follows: $\lambda_1 = \frac{(a-d)e^2+((a\eta-d)k-c)e-ck}{(k+e)e}$ and $\lambda_2 = -1 < 0$. Clearly, if $c < c^{**}$, then $\lambda_1 > 0$, indicating that E_2 is a saddle. Conversely, if $c > c^{**}$, then $\lambda_1 < 0$, making E_2 a stable node. When $c = c^{**}$, then $\lambda_1 = 0$, making E_2 a degenerate equilibrium. We translate $E_2(0,\frac{1}{e})$ to $(0,0)$ and expand around the origin up to the third order. We make the following transformation:

$$X = x,\ Y = y - \frac{1}{e},\ d\tau = -dt.$$

The resulting system (1.7) is:

$$\begin{cases} \dfrac{dX}{d\tau} = a_{20}X^2 + a_{11}XY + a_{30}X^3 + a_{21}X^2Y + a_{12}XY^2 + O(|X,Y|^3), \\ \dfrac{dY}{d\tau} = Y + eY^2, \end{cases} \tag{2.9}$$

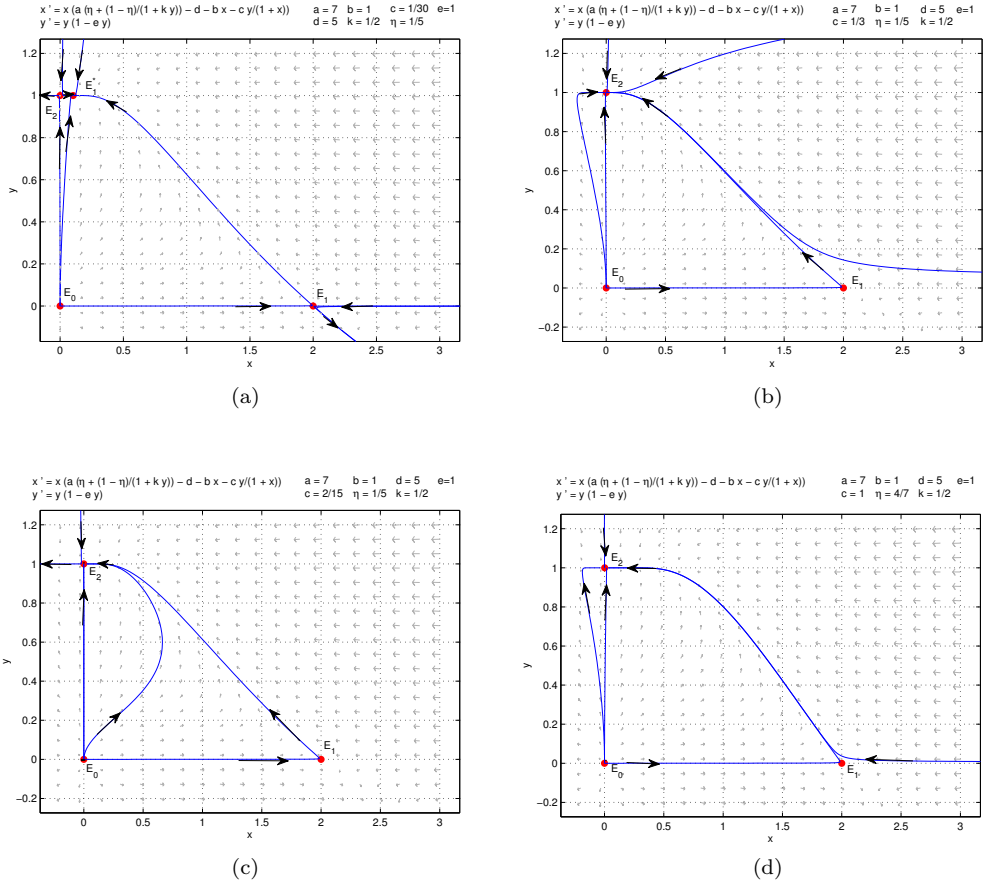

Figure 1. (a) $0 < c < c^{**}$, E_2 is a saddle; (b) $c > c^{**}$, E_2 is a stable node; (c) $c = c^{**}$ and $\eta \neq \eta^*$, E_2 is a attracting saddle-node; (d) $c = c^{**}$ and $\eta = \eta^*$, E_2 is a degenerate stable node.

where

$$a_{20} = \frac{be - c^{**}}{e},\ a_{30} = \frac{c^{**}}{e},\ a_{21} = -c^{**},\ a_{12} = \frac{a\,(-1+\eta)\,e^3k^2}{(k+e)^3},$$

$$a_{11} = \frac{ae^2k\eta - ae^2k - c^{**}e^2 - 2c^{**}ek - c^{**}k^2}{(k+e)^2}.$$

Utilizing the central manifold theorem, with the assumption $Y = mX^2 + nX^3 + O(|X|^3)$, substitute this expression into the second equation of the system (2.9). We can achieve $Y = 0$. The constrained system limited to the central manifold is expressed as follows:

$$\frac{dX}{d\tau} = \frac{(be - c^{**})}{e}X^2 + \frac{c^{**}}{e}X^3 + O(X^3).$$

Now we consider the following cases.

Case 1. If $\frac{be-c^{**}}{e} > 0\ (< 0)$, i.e., $\eta < (>, resp.)\eta^*$, then $m = 2,\ a_m = a_{20} = \frac{(be-c^{**})}{e} > 0\ (< 0)$. Hence, according to Theorem 7.1 in Zhang [42], it shows that E_2 is an attracting saddle-node, with the parabolic sector located in the right (left) half-plane.

Case 2. If $\frac{be-c^{**}}{e} = 0$, i.e., $\eta = \eta^*$, then $m = 3,\ a_m = a_{30} = \frac{c^{**}}{e} > 0$. It shows that E_2 is a degenerate stable node of codimension 2.

The phase portraits in Figure 1 were generated using the MATLAB tool pplane [25], which simulates the dynamic behavior of the system(1.7) under the given parameter conditions.

The proof of Theorem 2.2 is completed. □

Theorem 2.3. *The stability of the positive equilibria for system* (1.7) *is shown below:*
(1) For $E_1^*(x_1^*, y^*)$*, when* E_1^* *exist (i.e.,* $0 < c \le c^{**}$ *or* $c^{**} < c < c^*$*,* $\eta > \eta^*$*),* E_1^* *is a stable node (Figure 2(a)-(b) [25]);*
(2) For $E_2^*(x_2^*, y^*)$*, when* E_2^* *exist (i.e.,* $c^{**} < c < c^*$ *and* $\eta > \eta^*$*),* E_2^* *is a saddle (Figure 2(b));*
(3) For $E_3^*(x_3^*, y^*)$*, when* E_3^* *exist (i.e.,* $c = c^*$ *and* $\eta > \eta^*$*),* E_3^* *is an attracting saddle-node (Figure 2(c)).*

Proof. Based on (2.5), the Jacobian matrix at E_i^* is

$$J(E_i^*) = \begin{pmatrix} A_i & x_i^*\left(-\dfrac{a(1-\eta)k}{(ky^*+1)^2} - \dfrac{c}{1+x_i^*}\right) \\ 0 & -1 \end{pmatrix}, \tag{2.10}$$

where $A_i = -bx_i^* + \frac{cx_i^*y^*}{(1+x_i^*)^2}$. The two eigenvalues of $J(E_i^*)$ are $\lambda_1 = A_i$ and $\lambda_2 = -1 < 0$. Thus, the stability of E_i^* is dependent upon the sign of A_i. We will examine this in three cases

Case 1. System (1.7) has only one positive equilibrium $E_1^*(x_1^*, y^*)$ (i.e., $0 < c \le c^{**}$).

Based on $a(\eta + \frac{1-\eta}{1+ky}) - d - bx - \frac{cy}{1+x} = 0$, we can get $-bx = -a(\eta + \frac{1-\eta}{1+ky}) + d + \frac{cy}{1+x}$. And at this time, $\eta > \eta^{**}$. Then

$$\begin{aligned} A_1(x_1^*, y^*) &= -bx_1^* + \frac{cx_1^*y^*}{(1+x_1^*)^2} \\ &= -a\left(\eta + \frac{1-\eta}{1+ky^*}\right) + d + \frac{cy^*}{1+x_1^*} + \frac{cx_1^*y^*}{(x_1^*+1)^2} \\ &\le -a\left(\eta + \frac{1-\eta}{1+ky^*}\right) + d + \frac{c^{**}y^*}{1+x_1^*} + \frac{c^{**}x_1^*y^*}{(x_1^*+1)^2} \\ &< -a\left(\eta^{**} + \frac{1-\eta^{**}}{1+ky^*}\right) + d + \frac{c^{**}y^*}{1+x_1^*} + \frac{c^{**}x_1^*y^*}{(x_1^*+1)^2} \\ &= 0. \end{aligned}$$

Thus, the eigenvalue is $\lambda_1 = A_1 < 0$, so E_1^* is a stable node.

Case 2. System (1.7) has two positive equilibria $E_1^*(x_1^*, y^*)$ and $E_2^*(x_2^*, y^*)$ (i.e., $c^{**} < c < c^*$ and $\eta > \eta^*$).

Let

$$A(x) := -a\left(\eta + \frac{1-\eta}{1+ky^*}\right) + d + \frac{cy^*}{1+x} + \frac{cxy^*}{(x+1)^2},\ x \in \left(0, \frac{a-d}{b}\right). \tag{2.11}$$

Obviously, we can obtain

$$\begin{aligned} \frac{dA(x)}{dx} &= \frac{d}{dx}\left(\frac{cy^*}{1+x}\right) + \frac{d}{dx}\left(\frac{cxy^*}{(x+1)^2}\right) \\ &= -\frac{cy^*}{(1+x)^2} + \frac{cy^*}{(1+x)^2} - \frac{2cxy^*}{(1+x)^3} \\ &= -\frac{2cxy^*}{(1+x)^3} \\ &< 0. \end{aligned} \tag{2.12}$$

It follows that $A(x)$ is monotonically decreasing in the interval $(0, \frac{a-d}{b})$.
Furthermore, since $c = c^*$, $x_3^* = \frac{(-b+a-d)e^2+k(a\eta-b-d)e}{2(be^2+bke)}$ and $y^* = \frac{1}{e}$, it can be concluded that

$$A(x_3^*) = -bx_3^* + \frac{c^* x_3^* y^*}{(1+x_3^*)^2} = 0. \tag{2.13}$$

According to the analysis above, since $0 < x_2^* < x_3^* < x_1^* < \frac{a-d}{b}$, it follows that $A(x_2^*) > 0$ and $A(x_1^*) < 0$. In this instance, one of the eigenvalues of $J(E_1^*)$ is $\lambda_1 = A_1 < 0$, so E_1^* is a stable node; one of the eigenvalues of $J(E_2^*)$ is $\lambda_1 = A_2 > 0$, so E_2^* is a saddle.

Case 3. System (1.7) has only one positive equilibrium $E_3^*(x_3^*, y^*)$ (i.e., $c = c^*$ and $\eta > \eta^*$) .

From (2.13), we obtain $A_3 = 0$, $J(E_3^*)$ has two eigenvalues: $\lambda_1 = 0$ and $\lambda_2 < 0$, E_3^* is degenerate, By using the transformation $d\tau = \frac{dt}{(1+ky)(1+x)}$, system (1.7) is reformulated as

$$\begin{cases} \dfrac{dx}{d\tau} = x\Big(a\eta(1+ky)(1+x) + a(1-\eta)(1+x) - (d+bx)(1+ky)(1+x) - cy(1+ky)\Big), \\ \dfrac{dy}{d\tau} = y(1-ey)(1+ky)(1+x). \end{cases} \tag{2.14}$$

Next, we translate $E_3^*(x_3^*, y^*)$ to $(0,0)$ and expand around the origin up to the third order. We apply the following transformations: $X = x - x_3^*$, $Y = y - y^*$. This enables us to rewrite system (2.14) as:

$$\begin{cases} \dfrac{dX}{d\tau} = a_{01}Y + a_{20}X^2 + a_{11}XY + a_{02}Y^2 + a_{30}X^3 + a_{21}X^2Y + a_{12}XY^2, \\ \dfrac{dY}{d\tau} = b_{01}Y + b_{11}XY + b_{02}Y^2 + b_{12}XY^2 + b_{03}Y^3, \end{cases} \tag{2.15}$$

where

$$\begin{aligned} a_{01} &= -x_3^*\left(bk\,x_3^* - a\eta k x_3^* + bkx_3^* + dkx_3^* + 2cky^* - a\eta k + dk + c\right), \\ a_{20} &= -3bkx_3^* y^* + a\eta k y^* - bk\,y^* - dky^* - 3bx_3^* + a - b - d, \\ a_{11} &= -3bk\,x_3^{*2} + 2a\eta k x_3^* - 2bkx_3^* - 2dkx_3^* - 2cky^* + a\eta k - dk - c, \\ a_{02} &= -x_3^* ck,\ a_{30} = -\left(ky^* + 1\right)b,\ a_{21} = -k\left(3bx_3^* - a\eta + b + d\right), \\ a_{12} &= -ck,\ b_{01} = -(3eky^{*2} + 2ey^* - 2ky^* - 1)\left(x_3^* + 1\right), \\ b_{11} &= -3ek\,y^{*2} - 2ey^* + 2ky^* + 1, \\ b_{02} &= \left(-3eky^* - e + k\right)\left(x_3^* + 1\right), \\ b_{12} &= -3eky^* - e + k,\ b_{03} = -ek\left(x_3^* + 1\right). \end{aligned}$$

Next, by setting $(X_1, Y_1) = (X - \frac{a_{01}}{b_{01}}Y, Y)$, system (2.15) becomes

$$\begin{cases} \dfrac{dX_1}{d\tau} = a_{20}(X_1 + \frac{a_{01}}{b_{01}}Y_1)^2 + (a_{11} - \frac{a_{01}b_{11}}{b_{01}})(X_1 + \frac{a_{01}}{b_{01}}Y_1)Y_1 + (a_{02} - \frac{a_{01}b_{02}}{b_{01}})Y_1^2 \\ \qquad\quad + a_{30}(X_1 + \frac{a_{01}}{b_{01}}Y_1)^3 + a_{21}(X_1 + \frac{a_{01}}{b_{01}}Y_1)^2 Y_1 \\ \qquad\quad + (a_{12} - \frac{a_{01}b_{12}}{b_{01}})(X_1 + \frac{a_{01}}{b_{01}}Y_1)Y_1^2 - \frac{a_{01}b_{03}}{b_{01}}Y_1^3, \\ \dfrac{dY_1}{d\tau} = b_{01}Y_1 + b_{11}(X_1 + \frac{a_{01}}{b_{01}}Y_1)Y_1 + b_{02}Y_1^2 + b_{12}(X_1 + \frac{a_{01}}{b_{01}}Y_1)Y_1^2 + b_{03}Y_1^3. \end{cases} \tag{2.16}$$

Further, using the transfromation $dt = b_{01}d\tau$, system (2.16) is rewritten as

$$\begin{cases} \dfrac{dX_1}{dt} = P(X_1, Y_1), \\ \dfrac{dY_1}{dt} = Y_1 + Q(X_1, Y_1), \end{cases} \tag{2.17}$$

where

$$\begin{aligned} P(X_1, Y_1) =& \frac{a_{20}}{b_{01}}(X_1 + \frac{a_{01}}{b_{01}}Y_1)^2 + (\frac{a_{11}}{b_{01}} - \frac{a_{01}b_{11}}{b_{01}^2})(X_1 + \frac{a_{01}}{b_{01}}Y_1)Y_1 + (\frac{a_{02}}{b_{01}} - \frac{a_{01}b_{11}}{b_{01}^2})Y_1^2 \\ &+ \frac{a_{30}}{b_{01}}(X_1 + \frac{a_{01}}{b_{01}}Y_1)^3 + \frac{a_{21}}{b_{01}}(X_1 + \frac{a_{01}}{b_{01}}Y_1)^2Y_1 \\ &+ (\frac{a_{12}}{b_{01}} - \frac{a_{01}b_{11}}{b_{01}^2})(X_1 + \frac{a_{01}}{b_{01}}Y_1)Y_1^2 - \frac{a_{01}b_{03}}{b_{01}^2}Y_1^3, \\ Q(X_1, Y_1) =& Y_1 + \frac{b_{11}}{b_{01}}(X_1 + \frac{a_{01}}{b_{01}}Y_1)Y_1 + \frac{b_{02}}{b_{01}}Y_1^2 + \frac{b_{12}}{b_{01}}(X_1 + \frac{a_{01}}{b_{01}}Y_1)Y_1^2 + \frac{b_{03}}{b_{01}}Y_1^3. \end{aligned}$$

Utilizing the central manifold theorem, with the assumption $Y_1 = mX_1^2 + nX_1^3 + O(|X_1|^3)$, substitute this expression into the second equation of the system (2.17). We can derive $Y_1 = 0$. The constrained system limited to the central manifold is expressed as follows

$$\frac{dX_1}{dt} = \frac{a_{20}}{b_{01}}X_1^2 + \frac{a_{30}}{b_{01}}X_1^3.$$

Since $\eta > \eta^*$, it is therefore evident that $m = 2$ and

$$a_m = \frac{a_{20}}{b_{01}} = \frac{b\left((-b + a - d)\, e + k\,(a\eta - b - d)\right)}{(b + a - d)\, e + k(a\eta + b - d)} > 0.$$

Theorem 7.1 in Zhang [42] demonstrates that E_3^* is an attracting saddle-node, with the parabolic sector located in the right half-plane.

The proof of Theorem 2.3 is completed. □

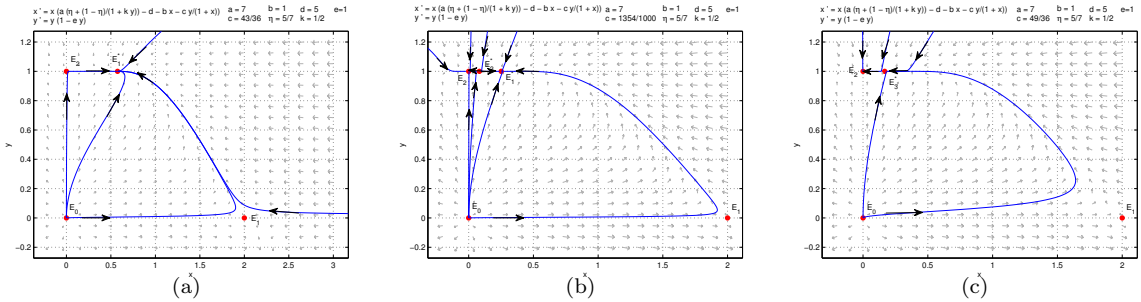

(a) (b) (c)

Figure 2. (a) $0 < c \le c^{**}$, E_1^* is a stable node; (b) $c^{**} < c < c^*$ and $\eta > \eta^*$, E_1^* is a stable node and E_2^* is a saddle; (c) $c = c^*$ and $\eta > \eta^*$, E_3^* is an attracting saddle-node.

Table 1 delineates the local dynamical characteristics of the equilibria of system (1.7). The number and stability of equilibria fluctuate based on the spectrum of parameter values.

Consequently, we partition $(a, b, c, d, e, k, \eta) \in R_7^+$ into four distinct regions.

$$\begin{aligned}
G_1 =& G_{11} \cup G_{12} \\
=& \{(a, b, c, d, e, k, \eta) \in R_7^+ : c^{**} \leq c \leq c^*,\ \eta \leq \eta^*\} \\
& \cup \{(a, b, c, d, e, k, \eta) \in R_7^+ : c > c^*\}, \\
G_2 =& G_{21} \cup G_{22} \\
=& \{(a, b, c, d, e, k, \eta) \in R_7^+ : 0 < c < c^{**}\} \\
& \cup \{(a, b, c, d, e, k, \eta) \in R_7^+ : c = c^{**},\ \eta > \eta^*\}, \\
G_3 =& \{(a, b, c, d, e, k, \eta) \in R_7^+ : c = c^*,\ \eta > \eta^*\}, \\
G_4 =& \{(a, b, c, d, e, k, \eta) \in R_7^+ : c^{**} < c < c^*,\ \eta > \eta^*\}.
\end{aligned}$$

Table 1. Stability of equilibria in system (1.7) under different parameter conditions.

Equilibrium	Existence		Stability
$E_0(0,0)$	Always exists		unstable
$E_1(\frac{a-d}{b}, 0)$	$a > d$		saddle
$E_2(0, \frac{1}{e})$	Always exists	$\eta > \eta^{**}$, $d < a < \frac{(k+e)d}{e}$	$0 < c < c^{**}$, saddle
			$c > c^{**}$, stable node
			$c = c^{**}$, $\eta \neq \eta^*$, attracting saddle-node
			$c = c^{**}$, $\eta = \eta^*$, stable node
$E_1^*(x_1^*, y^*)$	$0 < c \leq c^{**}$, $\eta > \eta^{**}$, $d < a < \frac{(k+e)(b+d)}{e}$		stable node
	$c^{**} < c < c^*$, $\eta > \eta^*$, $b + d < a < \frac{d(k+e)}{e}$, $k > \frac{eb}{d}$		
$E_2^*(x_2^*, y^*)$	$c^{**} < c < c^*$, $\eta > \eta^*$, $b + d < a < \frac{d(k+e)}{e}$, $k > \frac{eb}{d}$		saddle
$E_3^*(x_3^*, y^*)$	$c = c^*$, $\eta > \eta^*$, $b + d < a < \frac{(k+e)(b+d)}{e}$		attracting saddle-node

For $G_1 = G_{11} \cup G_{12}$, There are three equilibria E_0, E_1 and E_2 in system (1.7). In the first quadrant E_0 and E_1 are saddle points, while E_2 is a stable node.

For $G_2 = G_{21} \cup G_{22}$, There are four equilibria E_0, E_1, E_2 and E_1^* in system (1.7). Both E_0 and E_1 are saddle points, and E_1^* is a stable node. In G_{21}, E_2 is a saddle, and in G_{22}, E_2 is an attracting saddle-node.

For G_3, There are four equilibria E_0, E_1, E_2 and E_3^* in system (1.7). In the first quadrant E_0 and E_1 are saddle points, E_2 is a stable node, while E_3^* is an attracting saddle-node.

For G_4, There are five equilibria E_0, E_1, E_2, E_1^* and E_2^* in system (1.7). In the first quadrant E_0 , E_1 and E_2^* are saddle points, while E_2 and E_1^* are stable nodes.

The qualitative characteristics of the equilibria in regions G_1, G_2, G_3 and G_4 are illustrated in Figure 3.

Remark 2.3. From Table 1, it can be inferred that c^{**} serves as the critical value for the stability of E_2 and the existence of E_2^*. This indicates that when $c > c^{**}$, a positive equilibrium E_2^* exists, suggesting coexistence of the two species. Conversely, when $c < c^{**}$, E_2^* disappears, and E_2 transitions from a stable node to a saddle in the first quadrant.

2.3. Bifurcation analysis

2.3.1. Transcritical bifurcation

Based on Theorems 2.2 and 2.3, an intriguing occurrence is noted: when $c = c^{**}$, $\eta^{**} < \eta < \eta^*$, the boundary equilibrium E_2 of system (1.7) coincides with the positive equilibrium E_1^*. And

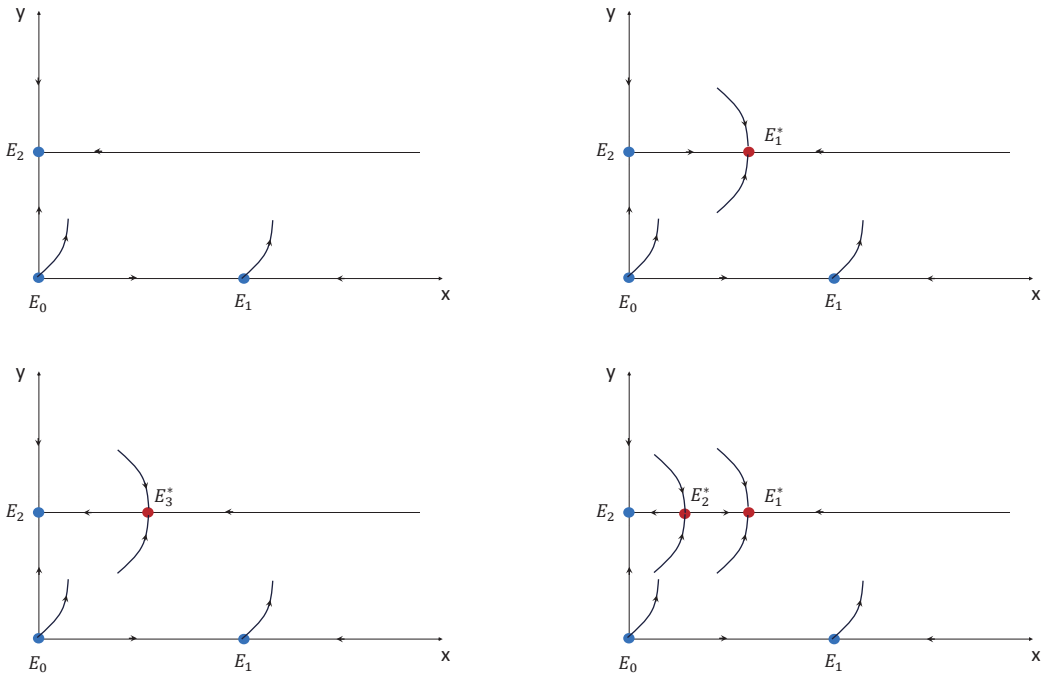

Figure 3. The qualitative properties of the equilibria for G_1, G_2, G_3 and G_4.

When $c < c^{**}$, E_2 is a saddle; when $c > c^{**}$, E_2 is a stable node, indicating that the stability of E_2 changes at $c = c^{**}$. This transpires as a result of a transcritical bifurcation at E_2.

Theorem 2.4. *Transcritical bifurcation of system* (1.7) *occurs at* E_2 *when* $c = c^{**}$ *and* $\eta < \eta^*$. $c \equiv c^{**} = \frac{e(a\eta k + ea - de - dk)}{k+e}$ *is the value in this case.*

Proof. When $c = c^{**}$ and $\eta < \eta^*$, the Jacobian matrix at E_2 is

$$J_{E_2}(x_2, y^*; c^{**}) = \begin{pmatrix} 0 & 0 \\ 0 & -1 \end{pmatrix}.$$

Clearly, $Det(J_{E_2}) = 0$, indicating that J_{E_2} possesses the eigenvalues $\lambda_1 = 0$, $\lambda_2 = -1$. Define v and w as the eigenvectors of $\lambda_1 = 0$ for J_{E_2} and $J_{E_2}^T$, respectively. We can obtain that

$$v = \begin{pmatrix} v_1 \\ v_2 \end{pmatrix} = \begin{pmatrix} 1 \\ 0 \end{pmatrix}, \ w = \begin{pmatrix} w_1 \\ w_2 \end{pmatrix} = \begin{pmatrix} 1 \\ 0 \end{pmatrix}. \tag{2.18}$$

Denote

$$Q = \begin{pmatrix} F \\ G \end{pmatrix} = \begin{pmatrix} x\left(a(\eta + \dfrac{1-\eta}{1+ky}) - d - bx - \dfrac{cy}{1+x}\right) \\ y(1-ey) \end{pmatrix}. \tag{2.19}$$

Furthermore, we have

$$Q_c(E_2;c^{**}) = \begin{pmatrix} \dfrac{\partial F}{\partial c} \\ \dfrac{\partial G}{\partial c} \end{pmatrix}_{(0,\frac{1}{e})} = \begin{pmatrix} \dfrac{-xy}{1+x} \\ 0 \end{pmatrix}_{(0,\frac{1}{e})} = \begin{pmatrix} 0 \\ 0 \end{pmatrix}, \tag{2.20}$$

$$DQ_c(E_2;c^{**})v = \begin{pmatrix} -\dfrac{y}{(x+1)^2} & 0 \\ 0 & 0 \end{pmatrix}_{(E_2;c^{**})} \begin{pmatrix} 1 \\ 0 \end{pmatrix} = \begin{pmatrix} -\dfrac{1}{e} \\ 0 \end{pmatrix}, \tag{2.21}$$

$$\begin{aligned} D^2Q(E_2;c^{**})(v,v) &= \begin{pmatrix} \dfrac{\partial^2 F}{\partial x^2}v_1^2 + 2\dfrac{\partial^2 F}{\partial x\partial y}v_1v_2 + \dfrac{\partial^2 F}{\partial y^2}v_2^2 \\ \dfrac{\partial^2 G}{\partial x^2}v_1^2 + 2\dfrac{\partial^2 G}{\partial x\partial y}v_1v_2 + \dfrac{\partial^2 G}{\partial y^2}v_2^2 \end{pmatrix}_{(E_2;c^{**})} \\ &= \begin{pmatrix} -2b + \dfrac{2cy}{(1+x)^2} - \dfrac{2cxy}{(1+x)^3} \\ 0 \end{pmatrix}_{(E_2;c^{**})} \\ &= \begin{pmatrix} \dfrac{(-2b+2a-2d)e + 2k(a\eta - b - d)}{e+k} \\ 0 \end{pmatrix}. \end{aligned} \tag{2.22}$$

Since $\eta \neq \eta^*$, it follows from (2.20)–(2.22) that

$$\begin{aligned} &w^T Q_c(E_2;c^{**}) = 0, \\ &w^T[DQ_c(E_2;c^{**})v] = -\frac{1}{e} \neq 0, \\ &w^T[D^2Q(E_2;c^{**})(v,v)] = \frac{(-2b+2a-2d)e + 2k(a\eta - b - d)}{e+k} \neq 0. \end{aligned} \tag{2.23}$$

According to Sotomayor's Theorem [24], when $c = c^{**}$ and $\eta < \eta^*$, system (1.7) experiences a transcritical bifurcation at E_2.

The proof of Theorem 2.4 is completed. □

The diagram of the transcritical bifurcation around E_2 when $c = c^{**}$ is shown in Figure 4(a)-(c). [25]

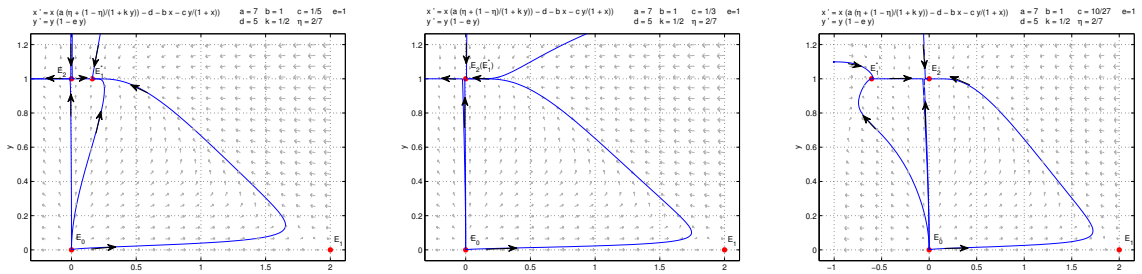

Figure 4. System (1.7) experiences a transcritical bifurcation at E_2.

2.3.2. Pitchfork bifurcation

According to Theorem 2.4, when $\eta = \eta^*$, the third transversality condition for the transcritical bifurcation at E_2 is given by (2.23) equals to zero. Furthermore, E_2 becomes a degenerate stable node when $c = c^{**}$ and $\eta = \eta^*$. By fixing $\eta = \eta^*$, as the parameter c varies, the positive equilibria E_1^* and E_2^* will converge with E_2. This is due to the bifurcation at E_2 created by the pitchfork bifurcation.

Theorem 2.5. *Pitchfork bifurcation of system* (1.7) *occurs at* E_2 *when* $c = c^{**}$ *and* $\eta = \eta^*$. *In this case,* $c^{**} = \frac{e(ak\eta+ea-ed-dk)}{k+e}$, $\eta^* = \frac{be+bk+de+dk-ea}{ka}$.

Proof. From (2.23), we have

$$w^T Q_c(E_2; c^{**}) = 0,$$
$$w^T [DQ_c(E_2; c^{**})v] = -\frac{1}{e} \neq 0,$$

when $\eta = \eta^*$, we obtain

$$w^T [D^2 Q(E_2; c^{**})(v, v)] = \frac{(-2b + 2a - 2d)e + 2k(a\eta - b - d)}{e + k} = 0.$$

By simple calculation, we ascertain

$$D^3 Q(E_2; c^{**})(v, v, v) = \begin{pmatrix} \frac{\partial^3 F}{\partial x^3} v_1^3 + \frac{\partial^3 F}{\partial x^2 \partial y} v_1^2 v_2 + \frac{\partial^3 F}{\partial x \partial y^2} v_1 v_2^2 + \frac{\partial^3 F}{\partial y^3} v_2^3 \\ \frac{\partial^3 G}{\partial x^3} v_1^3 + \frac{\partial^3 G}{\partial x^2 \partial y} v_1^2 v_2 + \frac{\partial^3 G}{\partial x \partial y^2} v_1 v_2^2 + \frac{\partial^3 G}{\partial y^3} v_2^3 \end{pmatrix}_{(E_2; c^{**})} \tag{2.24}$$
$$= \begin{pmatrix} -\frac{24b^3(e+k)^2}{((a\eta + b - d)k + e(b + a - d))^2} \\ 0 \end{pmatrix}.$$

Obviously,

$$w^T [D^3 Q(E_2; c^{**})(v, v, v)] = -\frac{24b^3(e+k)^2}{((a\eta + b - d)k + e(b + a - d))^2} \neq 0.$$

Sotomayor's Theorem [24] states that system (1.7) experiences a pitchfork bifurcation at E_2 when $c = c^{**}$ and $\eta = \eta^*$.

The proof of Theorem 2.5 is completed. □

The diagram of the pitchfork bifurcation around E_2 when $\eta = \eta^*$ is shown in Figure 5(a)-(c). [25]

2.3.3. Saddle-node bifurcation

Based on Theorem 2.1, when $\eta > \eta^*$, the system (1.7) exhibits no equilibrium for $c > c^*$, one positive equilibrium E_3^* for $c = c^*$, and two positive equilibria E_1^* and E_2^* for $c < c^*$. Thus, we determine that a saddle-node bifurcation takes place at E_3^* in system (1.7).

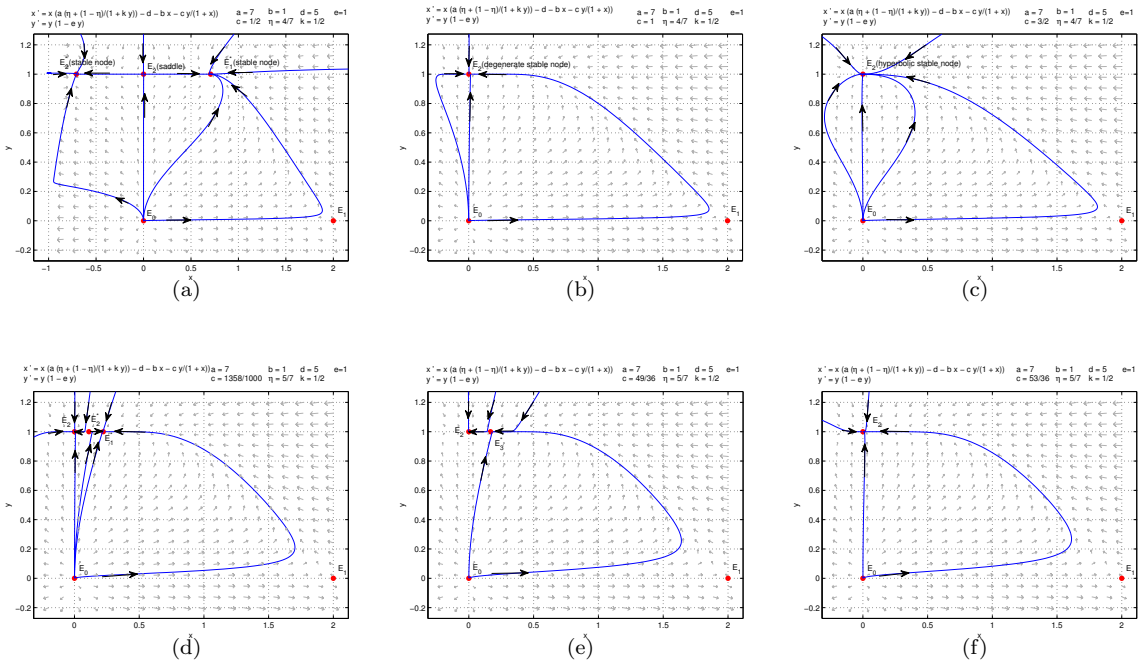

Figure 5. In (a)-(c), system (1.7) experiences a pitchfork bifurcation at E_2; In (d)-(f), system (1.7) experiences a saddle-node bifurcation at E_3^*.

Theorem 2.6. *Saddle-node bifurcation of system* (1.7) *occurs at* E_3^* *when* $c = c^*$ *and* $\eta > \eta^*$. *The bifurcation parameter* c *is defined as follows:*

$$c \equiv c^* = \frac{e(a\eta k + be + bk + ea - de - dk)^2}{4b(k+e)^2}.$$

Proof. When $c = c^*$, the Jacobian matrix at E_3^* is

$$J_{E_3^*}(x_3^*, y^*; c^*) = \begin{pmatrix} 0 & x_3^*\left(-\dfrac{a(1-\eta)k}{(ky^*+1)^2} - \dfrac{c}{1+x_3^*}\right) \\ 0 & -1 \end{pmatrix}.$$

Obviously, $Det(J_{E_3^*}) = 0$, indicating that $J_{E_3^*}$ possesses the eigenvalues $\lambda_1 = 0,\ \lambda_2 = -1$. Define V and W as the eigenvectors for $\lambda_1 = 0$ in $J_{E_3^*}$ and $J_{E_3^*}^T$, respectively. Then, they can be given by

$$V = \begin{pmatrix} V_1 \\ V_2 \end{pmatrix} = \begin{pmatrix} 1 \\ 0 \end{pmatrix},\ W = \begin{pmatrix} W_1 \\ W_2 \end{pmatrix} = \begin{pmatrix} 1 \\ x_3^*\left(\dfrac{a(1-\eta)k}{(ky^*+1)^2} + \dfrac{c}{1+x_3^*}\right) \end{pmatrix}. \tag{2.25}$$

Furthermore, one has

$$Q_c(E_3^*; c^*) = \begin{pmatrix} \dfrac{\partial F}{\partial c} \\ \dfrac{\partial G}{\partial c} \end{pmatrix}_{(x_3^*, y^*)} = \begin{pmatrix} -\dfrac{x_3^* y^*}{1+x_3^*} \\ 0 \end{pmatrix}, \tag{2.26}$$

$$D^2Q(E_3^*;c^*)(V,V)=\begin{pmatrix}\dfrac{\partial^2F}{\partial x^2}V_1^2+2\dfrac{\partial^2F}{\partial x\partial y}V_1V_2+\dfrac{\partial^2F}{\partial y^2}V_2^2\\ \dfrac{\partial^2G}{\partial x^2}V_1^2+2\dfrac{\partial^2G}{\partial x\partial y}V_1V_2+\dfrac{\partial^2G}{\partial y^2}V_2^2\end{pmatrix}_{(E_3^*;c^*)}=\begin{pmatrix}N\\0\end{pmatrix},\tag{2.27}$$

where

$$N=-\frac{2b((-b+a-d)e+k(a\eta-b-d))}{(b+a-d)e+k(a\eta+b-d)}.$$

Since $\eta\neq\eta^*$, it follows from (2.26)–(2.27) that

$$W^TQ_c(E_3^*;c^*)=-\frac{x_3^*y^*}{1+x_3^*}\neq 0,$$
$$W^T[D^2Q(E_3^*;c^*)(V,V)]=N\neq 0.$$

Sotomayor's Theorem [24] states that system (1.7) experiences a saddle-node bifurcation at E_3^* when $c=c^*$ and $\eta>\eta^*$.

The proof of Theorem 2.6 is completed. □

The diagram of the saddle-node bifurcation around E_3^* when $c=c^*$ is shown in Figure 5(d)-(f). [25]

Remark 2.4. The saddle-node bifurcation reveals the critical value of the influencing factor c (the negative impact of the second species on the first species). When c exceeds this critical value, the first species cannot maintain its stability and will eventually go extinct. This phenomenon provides a theoretical basis for understanding the extinction threshold of species under amensalism. The transcritical bifurcation reveals the combined effect of the influencing factor c and the saturated fear parameter η on population stability. When η is low, the fear effect has a greater negative impact on the first species, making the first species more prone to extinction. This phenomenon offers an important perspective for understanding the regulatory role of the fear effect in the amensalism system. The pitchfork bifurcation reveals the regulatory effect of the saturated fear parameter η on population dynamics. When η exceeds a certain threshold, the saturation characteristic of the fear effect can alleviate its negative impact on the first species and promote the stable co-existence of the two species.

2.4. Global structure

2.4.1. The dynamics near infinity

To understand the overall behavior of system (1.7) and gain insights into the trajectory patterns as $|x|+|y|\to\infty$, we will examine the stability at infinity by applying standard Poincaré sphere techniques, as outlined in Chapter 5 of the reference Zhang [42]:

$$x=\frac{v}{z},\ y=\frac{1}{z},\ ds=\frac{dt}{z},$$

system (1.7) can be transformed into

$$\begin{cases}\dfrac{dv}{ds}=avz\left(\eta+\dfrac{(1-\eta)z}{z+k}\right)-dvz-vz+(e-bv)\,v-\dfrac{cvz}{z+v},\\ \dfrac{dz}{ds}=ez-z^2.\end{cases}\tag{2.28}$$

With $z = 0$, system (2.28) exists two equilibria $D_0(0,0)$ and $D_1(\frac{e}{b},0)$ in the first quadrant of $v - z$ plane.

Next, we apply the second type of Poincaré transformation:

$$x = \frac{1}{z},\ y = \frac{u}{z},\ ds = \frac{dt}{z},$$

system (1.7) becomes

$$\begin{cases} \dfrac{du}{ds} = auz\left(\eta + \dfrac{z(1-\eta)}{z+ku}\right) + duz + bu + \dfrac{cu^2z}{1+z} + zu - eu^2, \\ \dfrac{dz}{ds} = az^2\left(\eta + \dfrac{z(1-\eta)}{z+ku}\right) + dz^2 + bz + \dfrac{cu^2z}{1+z}. \end{cases} \tag{2.29}$$

Obviously, system (2.29) exists one boundary equilibrium $D_2(0,0)$ in the first quadrant of $u - z$ plane.

Theorem 2.7. *In system* (2.28), $D_0(0,0)$ *is an unstable node and* $D_1(\frac{e}{b},0)$ *is a saddle. In system* (2.29), $D_2(0,0)$ *is an unstable node.*

Proof. The Jacobian matrices of system (2.28) at equilibria $D_0(0,0)$ and $D_1(\frac{e}{b},0)$ are

$$J(D_0) = \begin{pmatrix} e & 0 \\ 0 & e \end{pmatrix}, \quad J(D_1) = \begin{pmatrix} -e & \dfrac{(a\eta - d - 1)e - bc}{b} \\ 0 & e \end{pmatrix}. \tag{2.30}$$

Obviously, D_0 is an unstable node and D_1 is a saddle.

The Jacobian matrices of system (2.29) at equilibrium $D_2(0,0)$ is

$$J(D_2) = \begin{pmatrix} b & 0 \\ 0 & b \end{pmatrix}. \tag{2.31}$$

Obviously, D_3 is an unstable node. □

By combining Theorem 2.7 with the Poincaré transformation from Chapter 5 of Zhang [42], it is straightforward to conclude that D_1 represents the infinite points I in system (1.7), which are saddles. D_0 and D_2 correspond to the infinite points I_1 and I_2 respectively, which are unstable nodes. Subsequently, we illustrate the dynamics near infinity of system (1.7) in Figure 6.

Theorem 2.8. *System* (1.7) *has no closed orbit in* R_+^2.

The proof can be found in Theorem 2.7 of Guan & Chen [10].

From Theorem 2.2, Theorem 2.3 and Table 1, when system (1.7) meets the condition $0 < c < c^{**}$, all border equilibria are unstable, and there exists a singular stable positive equilibrium E_1^*. Moreover, when $c > c^{**}$ and $\eta \le \eta^*$, the system (1.7) lacks positive equilibrium; E_2 demonstrates local asymptotic stability, while E_0 and E_1 are unstable. Theorem 2.8 demonstrates that system (1.7) cannot possess a closed orbit in the positive quadrant, allowing us to formulate the subsequent theorems.

Theorem 2.9. *The boundary equilibrium* E_2 *is globally asymptotically stable when* $c > c^{**}$ *and* $\eta \le \eta^*$.

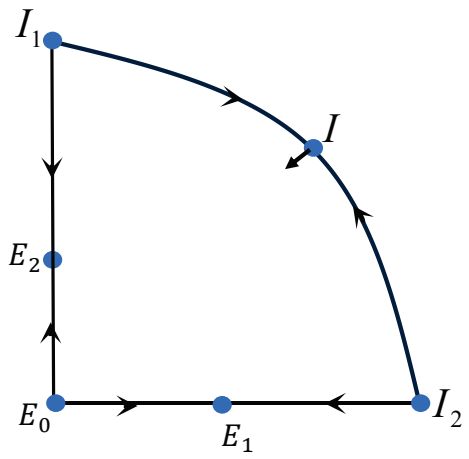

Figure 6. The dynamics of system (1.7) near infinity.

Theorem 2.10. *The locally stable positive equilibrium E_1^* is globally asymptotically stable when $0 < c < c^{**}$.*

Remark 2.5. When the influencing factor c is small, the negative impact of the second species on the first species is weak, enabling the first species to maintain a relatively high population density. The combined effect of the saturated fear effect and the Allee effect further alleviates the negative impact of fear on the first species, thus promoting the stable coexistence of the two species. When the influencing factor c is at an intermediate level, the system exhibits bistable behavior, indicating that the ecosystem may manifest two different stable states depending on the initial density. When the influencing factor c is large, the negative impact of the second species on the first species is strong, preventing the first species from maintaining population stability and ultimately leading to its extinction. This phenomenon reveals the critical value of the influencing factor c, providing a theoretical basis for understanding the extinction threshold of species under amensalism.

2.4.2. Global phase portraits

Theorem 2.7 previously established that system (1.7) has one equilibrium at infinity: I, corresponding to a saddle. Additionally, based on Theorem 2.8, system (1.7) does not exhibit any closed orbits. Consequently, we can now depict the complete global phase portraits for system (1.7).

To simplify notation, we represent the unstable manifolds of E_1 and I with the symbols φ_1 and φ_2, respectively. The ω-limit sets of φ_1 and φ_2 are represented by $\omega(\varphi_1)$ and $\omega(\varphi_2)$.

For parameter values $(a, b, c, d, k, \eta, e) \in G_1$, it can be easily verified that both $\omega(\varphi_1)$ and $\omega(\varphi_2)$ converge to E_2, as depicted in Figure 7.

For parameter values $(a, b, c, d, k, \eta, e) \in G_2$, both $\omega(\varphi_1)$ and $\omega(\varphi_2)$ converge to E_1^*, as depicted in Figure 8.

For parameters values $(a, b, c, d, k, \eta, e) \in G_3$, it is evident that $\omega(\varphi_1)$ and $\omega(\varphi_2)$ may correspond to either E_2 or E_3^*, potentially leading to scenarios depicted in Figure 9(a)-(i). To determine the feasibility of these nine cases, we must analyze the existence conditions for heteroclinic bifurcations. Focusing first on $\omega(\varphi_1)$, Figure 11(a) presents the system's (1.7) nullcline

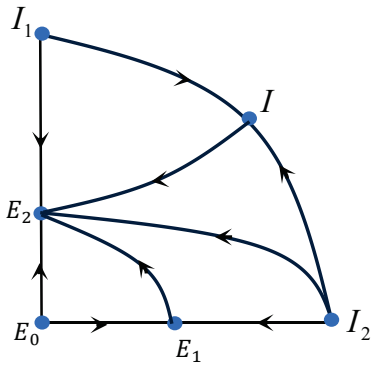

Figure 7. Global phase portraits of the system (1.7) in G_1.

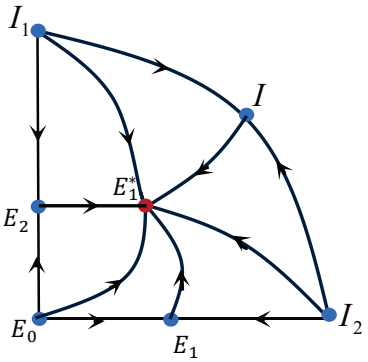

Figure 8. Global phase portraits of the system (1.7) in G_2.

structure when $c = c^*$, showing that trajectories in region III ($dx/dt < 0$, $dy/dt > 0$) cannot enter region II ($dx/dt > 0$, $dy/dt > 0$) as $t \to \infty$. This topological constraint necessitates that any trajectory φ_1 initiating in region III must asymptotically approach E_3^* while remaining within its own region, thereby establishing $\omega(\varphi_1) = E_3^*$. Consequently, the dynamical scenarios (d)-(i) depicted in Figure 9 are topologically impossible under these conditions.

Next, we consider $\omega(\varphi_2)$. Suppose that $\bar{c} > \tilde{c}$, since that $y > \frac{1}{e}$, we have

$$\begin{vmatrix} x\left(a(\eta + \dfrac{1-\eta}{1+ky}) - d - bx - \dfrac{\tilde{c}y}{1+x}\right) & y(1-ey) \\ x\left(a(\eta + \dfrac{1-\eta}{1+ky}) - d - bx - \dfrac{\bar{c}y}{1+x}\right) & y(1-ey) \end{vmatrix} = \frac{(\bar{c}-\tilde{c})xy^2(1-ey)}{1+x} < 0.$$

We derive the rotational behavior of the vector field associated with system (1.7) with respect to parameter c for $y \in \left(\frac{1}{e}, +\infty\right)$. According to Definition 3.3 in Chapter 4 of [42], the heteroclinic orbit φ_2 exhibits monotonic variation as parameter c increases. When a saddle connection exists, the heteroclinic bifurcation surface can be represented by the functional relation: $c = \varphi(a, b, c, d, e, k, \eta)$. Thus, the global phase portrait of system (1.7) in G_3 is shown in Figure 9(a)-(c).

For parameter values $(a, b, c, d, k, \eta, e) \in G_4$, it is clear that $\omega(\varphi_1)$ converges to E_3^* and $\omega(\varphi_2)$ to E_2. The specific analysis process is analogous to that for G_3. As illustrated in Figure 10, system (1.7) also exhibits three global phase portraits.

Remark 2.6. The singularities I at infinity in the first quadrant are unstable, leading to the interior equilibria E_i^* $(i = 1, 2, 3)$ or the border equilibrium E_2 (refer to Figures 8–10). Biologically speaking, although the initial densities of both species are quite high, their eventual densities decrease, leading either to stable coexistence or to the extinction of the first species while the second species persists.

3. Stochastic model of amensalism with saturation fear effect

Compared with previous studies, this paper pioneers the introduction of saturated fear effect in amensalism system, where the population x exhibits asymptotically saturated responses to fear effect (i.e., fear intensity approaches an upper threshold). Crucially, we demonstrate stable

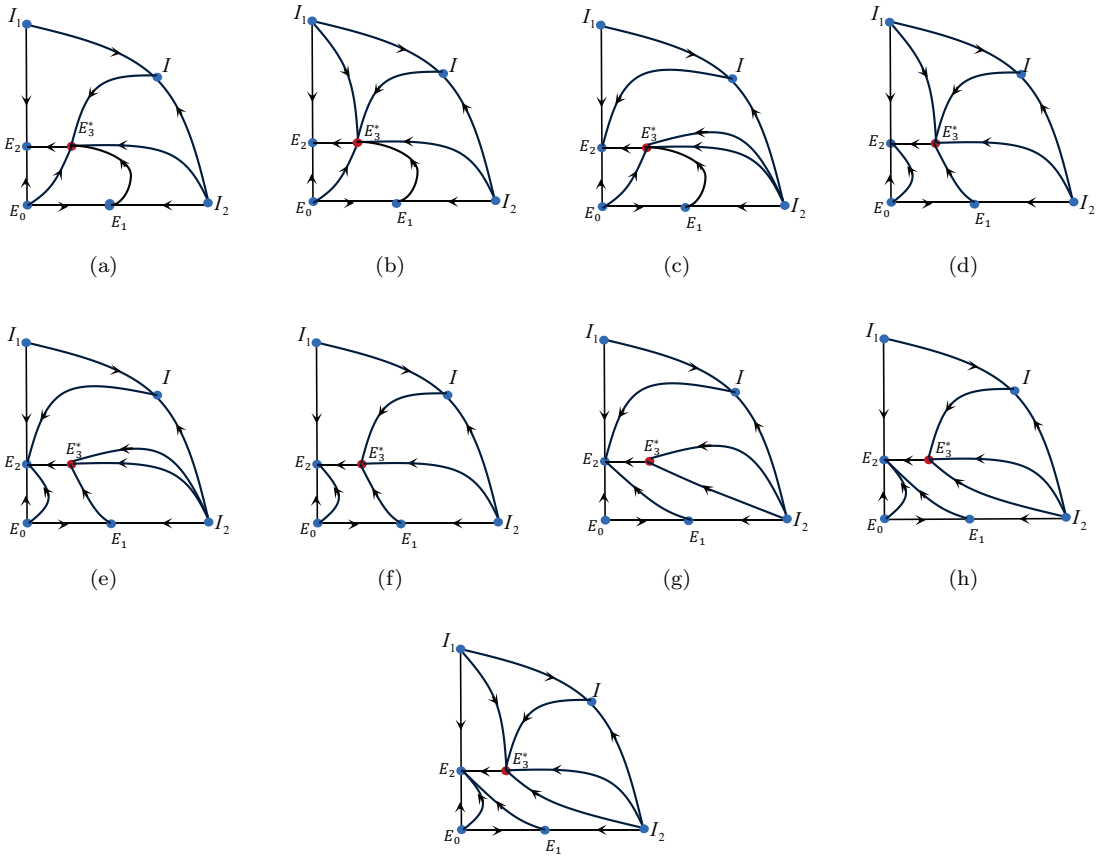

Figure 9. Global phase portraits of the system (1.7) in G_3.

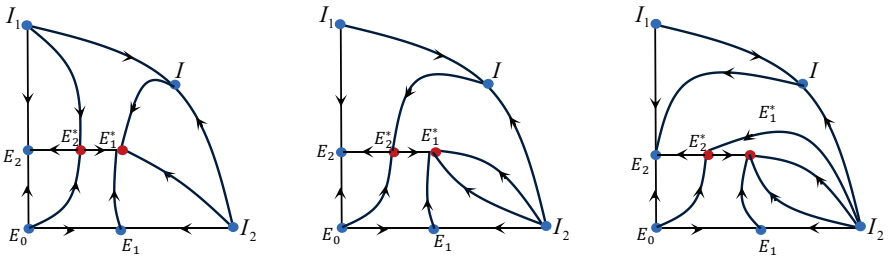

Figure 10. Global phase portraits of the system (1.7) in G_4.

coexistence of both species under specific conditions, making the survival analysis of population x particularly significant. As shown in Figure 2(b) and Table 1, when system parameters satisfy $c^{**} < c < c^*$ and $\eta > \eta^*$, the system (1.7) displays a distinctive bistable structure: two stable equilibria (E_2 and E_1^*) coexist, with the final state determined by initial population densities.

Environmental fluctuations, which are ubiquitous in ecosystems, exert significant impacts on population dynamics. For example, in Akimoto's [1] experiment, the elm aphid community may be affected by stochastic factors such as climate fluctuations. To quantify external disturbances on system (1.7), we incorporate multiplicative noise into key ecological parameters following

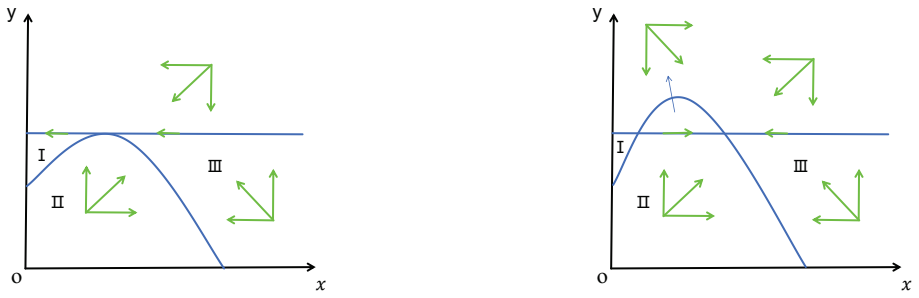

Figure 11. The horizontal isocline $\frac{dx}{dt} = 0$ and vertical isocline $\frac{dy}{dt} = 0$ of system (1.7).

Khasminskii's Theory [15]. The stochastic version of system (1.7) is formulated as [3, 12]:

$$a \to a + \sigma \dot{B}_1(t),\ 1 \to 1 + \sigma \dot{B}_2(t).$$

Here $B_1(t)$ and $B_2(t)$ are independent Brownian motions, with σ as noise intensities. The stochastic model becomes:

$$\begin{cases} dx = x\left(a\left(\eta + \dfrac{1-\eta}{1+ky}\right) - d - bx - \dfrac{cy}{1+x}\right)dt + \sigma x\left(\eta + \dfrac{1-\eta}{1+ky}\right)dB_1(t), \\ dy = y(1-ey)dt + \sigma y dB_2(t). \end{cases} \tag{3.1}$$

Subsequently, we analyze noise-induced impacts on the bistability of the stochastic system (3.1) via numerical simulations. Using stochastic sensitivity techniques, we construct confidence ellipses to estimate the critical noise threshold triggering transitions from coexistence to extinction.

Under the parameter configuration $(a, b, c, d, e, k, \eta) = (4, 1, 2, 1, 1, 1, \frac{1}{2})$, system (1.7) demonstrates distinct bistable behavior where the final steady state depends critically on initial conditions, as shown in Figure 12. When introducing weak noise ($\sigma = 0.05$) in the stochastic system (3.1), trajectories exhibit small fluctuations around the deterministic equilibrium without departing from their respective basins of attraction. We further investigate how noise intensity affects the system's steady states across different basins of attraction.

When selecting initial conditions $(0.05, 0.7)$, under weak noise ($\sigma = 0.07$ and $\sigma = 0.5$), solutions exhibit small oscillations around the deterministic equilibrium. As noise intensity increases to $\sigma = 1.5$, the system trajectory ultimately converges to E_0, indicating extinction of both populations. Notably, while noise does not alter population x's inevitable extinction outcome, stronger noise significantly accelerates its path to extinction. (see Figure 13)

When the initial condition is set to $(0.5, 0.4)$, under weak noise ($\sigma = 0.05$), the solutions oscillate stably around the deterministic equilibrium E_1^*, maintaining the coexistence state of both populations. As the noise increases to moderate levels ($\sigma = 0.3$), the system (3.1) undergoes a critical transition, trajectories escape the basin of attraction of E_1^* and converge to the boundary equilibrium E_2, where population x goes extinct while population y persists. When noise intensity further increases to $\sigma = 2.5$, the system (3.1) experiences complete collapse, with all trajectories ultimately approaching the extinction equilibrium E_0, indicating the annihilation of both populations. These results demonstrate the existence of multiple noise-induced tipping points in the system, where increasing environmental stochasticity can first trigger partial ecosystem degradation before leading to total system collapse. (see Figure 14)

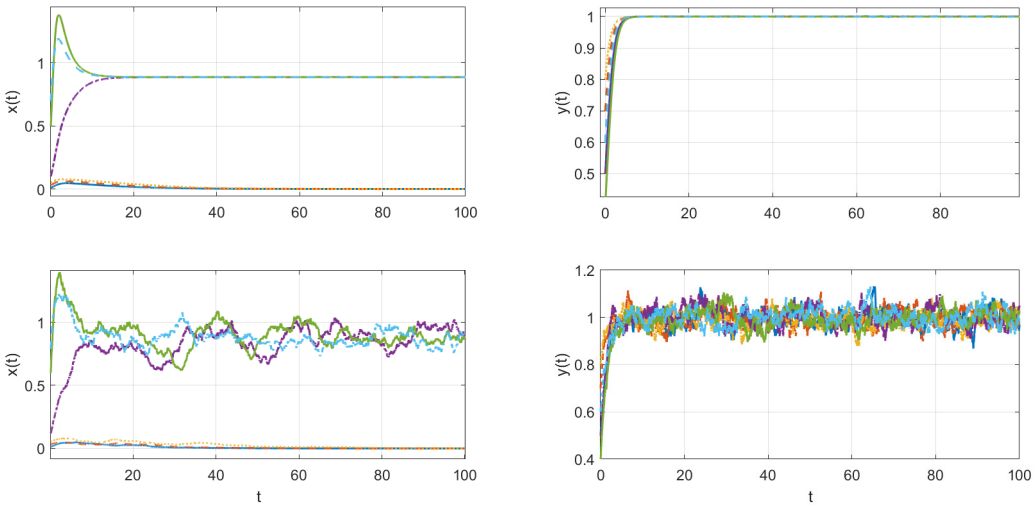

(a) (b)

Figure 12. Taking the intial values as $(0.01, 0.5), (0.03, 0.7), (0.05, 0.7), (0.2, 0.5), (0.5, 0.4), (0.8, 0.6))$, plot the time series of populations x and y for the deterministic system (1.7) and the stochastic system (3.1) with $\sigma = 0.05$.

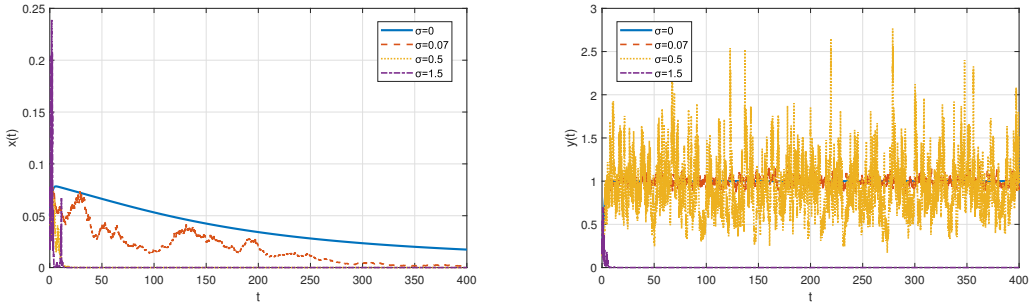

(a) (b)

Figure 13. Take the initial value as $(0.05, 0.7)$. When $\sigma = 0.07, 0.5, 1.5$, plot the time series of the two populations in the stochastic system (3.1).

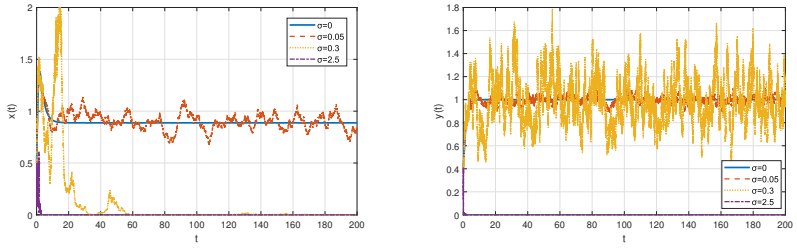

(a) (b)

Figure 14. Take the initial value as $(0.5, 0.4)$. When $\sigma = 0.05, 0.3, 2.5$, plot the time series of the two populations in the stochastic system (3.1).

The critical noise intensity (σ^*) serves as a crucial metric for assessing the stability of

stochastic systems, representing the maximum tolerable intensity of random perturbations. When environmental noise exceeds σ^*, the system exhibits a significant probability of escaping its current stable state (e.g., population extinction or state transition). In this study, we employ stochastic sensitivity techniques to construct confidence ellipses for estimating the critical noise threshold that triggers transitions from E_1^* to E_2 in the stochastic system (3.1). [3]

The Jacobian matrix $J(E_1^*)$ and diffusion matrix G are computed as follows:

$$J = \begin{pmatrix} j_{11} & j_{12} \\ j_{21} & j_{22} \end{pmatrix}, \ G = \begin{pmatrix} g_{11} & g_{12} \\ g_{21} & g_{22} \end{pmatrix},$$

where

$$j_{11} = x_1^*\left(-b + \frac{cx_1^*y^*}{(1+x_1^*)^2}\right), \ j_{12} = x_1^*\left(-\frac{a(1-\eta)k}{(ky^*+1)^2} - \frac{c}{1+x_1^*}\right), \ j_{21} = 0, \ j_{22} = -ey^*,$$
$$g_{11} = x_1^*\left(\eta + \frac{1-\eta}{1+ky^*}\right), \ g_{12} = 0, \ g_{21} = 0, \ g_{22} = y^*.$$

The stochastic sensitivity matrix

$$W = \begin{pmatrix} \omega_{11} & \omega_{12} \\ \omega_{21} & \omega_{22} \end{pmatrix}$$

is computed by solving the Lyapunov equation, where W satisfies $JW + WJ^T + GG^T = 0$ and is a positive definite matrix. Namely, it satisfies

$$\begin{cases} 2j_{11}\omega_{11} + j_{12}\omega_{12} + j_{12}\omega_{21} + g_{11}^2 = 0, \\ j_{21}\omega_{11} + (j_{11}+j_{22})\omega_{12} + j_{12}\omega_{22} = 0, \\ j_{21}\omega_{11} + (j_{11}+j_{22})\omega_{21} + j_{12}\omega_{22} = 0, \\ j_{21}\omega_{12} + j_{21}\omega_{21} + 2j_{22}\omega_{22} + g_{22}^2 = 0. \end{cases} \tag{3.2}$$

Construct a confidence ellipse

$$\langle (x-x_1^*, y-y^*)^T W^{-1}(x-x_1^*, y-y^*)\rangle = 2\sigma^2 \ln\left(\frac{1}{1-P}\right),$$

where $P = 0.95$, and σ is noise intensities.

Additionally, the separatrix is typically associated with the stable manifold of the unstable equilibrium E_2^*, dividing the basins of attraction between E_1^* and E_2. We gradually increase σ until it becomes tangent to the separatrix, the resulting σ value represents the critical noise threshold.

Next, we numerically verify the feasibility through simulation. Using the same parameter settings as in Figure 14, we obtain $E_1^* = (0.8873, 1)$. At this point, both the stochastic sensitivity matrix W and its inverse W^{-1} are

$$W = \begin{pmatrix} 2.6689 & -0.5245 \\ -0.5245 & 0.5 \end{pmatrix},$$

$$W^{-1} = \begin{pmatrix} 0.4720 & 0.4951 \\ 0.4951 & 2.5193 \end{pmatrix}.$$

Then, the corresponding confidence ellipse is

$$0.4720(x-0.8873)^2 + 0.99(x-0.8873)(y-1) + 2.5193(y-1)^2 = 2\sigma^2 \ln\left(\frac{1}{1-0.95}\right).$$

As shown in Figure 15, when the noise intensity is subcritical ($\sigma = 0.1$), the stochastic system (3.1) exhibits stable oscillations near the equilibrium E_1^*. Approximately 95% of the stochastic trajectories are confined within the confidence ellipse defined by the stochastic sensitivity matrix W (with a confidence level $P = 0.95$). The boundary between the basins of attraction of E_1^* and E_2 is sharply delineated by the separatrix $x = 0.1127$, which corresponds to the stable manifold of E_2^* in system (1.7), effectively separating the two attractors. When the noise intensity increases to the critical value $\sigma^* = 0.192$, the confidence ellipse becomes tangent to the separatrix $x = 0.1127$. This critical noise level $\sigma^* = 0.192$ marks the threshold for stochastic transitions between attractors. For supercritical noise levels ($\sigma = 0.5$), the system (3.1) trajectories initially linger near E_1^* before eventually being attracted into the basin of E_2. Thus, we have verified that $\sigma^* \approx 0.192$ represents the critical noise threshold for the transition from E_1^* to E_2 in the stochastic system (3.1).

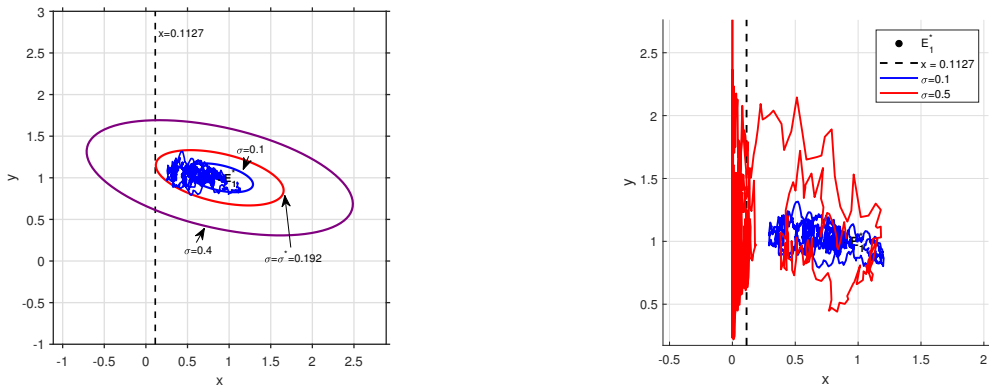

(a) (b)

Figure 15. Fix parameters $(a, b, c, d, e, k, \eta) = (4, 1, \frac{21}{10}, 1, 1, 1, \frac{1}{2})$. (a) Random states of system (3.1) when $\sigma = 0.1,$ and confidence ellipses of E_1^* for $\sigma = 0.1,\ 0.192$ and 0.4, respectively. (b) Random states of system (3.1) when $\sigma = 0.1,\ 0.5$, respectively.

In the deterministic system (1.7), when $\eta < \eta^*$ and the parameter satisfies $0 < c < c^{**}$, the system (1.7) exhibits equilibria E_2 and E_1^*. When $c = c^{**}$, E_1^* and E_2 collide and coincide, which we have proven in Section 2.3 to result from a transcritical bifurcation occurring at E_2 when $c = c^{**}$. In this section, by introducing stochastic perturbations to establish the stochastic system (3.1), numerical simulations (Figure 16) reveal that when $0 < c < c^{**}$, moderate noise ($\sigma = 0.5$) induces a state transition where a subset of solution trajectories originally converging to the coexistence equilibrium E_1^* are redirected toward the extinction equilibrium E_2. Furthermore, increasing noise intensity drives the system into a critical state prematurely. This phenomenon highlights the significant impact of stochastic perturbations on bifurcation thresholds, demonstrating that noise can induce state transitions even before the parameter reaches its deterministic critical value.

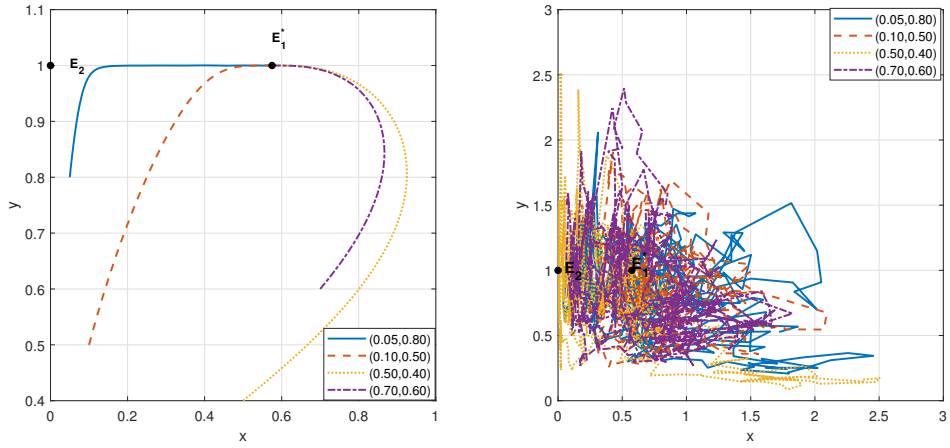

(a)

Figure 16. Fix parameters $(a, b, c, d, e, k, \eta) = (7, 1, \frac{43}{36}, 5, 1, \frac{1}{2}, \frac{5}{7})$, taking the initial values as $(0.05, 0.8), (0.1, 0.5), (0.5, 0.4), (0.7, 0.6)$), (a) phase portrait of system (1.7); (b) phase portrait of system (3.1) with $\sigma = 0.5$.

4. Global dynamics of system (1.9)

4.1. Analysis of equilibria

Theorem 4.1. *The existence of equilibria in system* (1.9) *is similar to that of system* (1.7). *However, the stability of the equilibria has undergone some changes. The qualitative properties of the equilibria in system* (1.9) *are presented in Table 2.*

Proof. The Jacobian matrix of system (1.9) at equilibrium (x, y) is

$$J(E) = \begin{pmatrix} H_1(x,y) & H_2(x,y) \\ 0 & H_3(x,y) \end{pmatrix}, \tag{4.1}$$

where

$$\begin{aligned} H_1(x,y) =& \frac{2x}{x+u}\left(a(\eta + \frac{1-\eta}{1+ky}) - d - bx - \frac{cy}{1+x}\right) + \frac{x}{x+u}\left(-bx + \frac{cxy}{(1+x)^2}\right) \\ & - \frac{x^2}{(x+u)^2}\left(a(\eta + \frac{1-\eta}{1+ky}) - d - bx - \frac{cy}{1+x}\right), \\ H_2(x,y) =& \frac{x^2}{x+u}\left(-\frac{ak(1-\eta)}{(1+ky)^2} - \frac{c}{1+x}\right), \quad H_3(x,y) = -2ey + 1. \end{aligned}$$

Here's a more concise and polished version of your passage while preserving all key mathematical and logical rigor:

Comparing with (2.5), H_1 has changed while H_3 remains unchanged. Direct calculation yields $H_1(0, y) = 0$, and since $a > d$, we derive $H_1\left(\frac{a-d}{b}, 0\right) = -\frac{(a-d)^2}{bu+a-d} < 0$. Consequently, relative to system (1.7), the stability of E_0 and E_2 has changed, whereas E_1 remains a saddle, as $H_3\left(\frac{a-d}{b}, 0\right) > 0$.

For the positive equilibria $E_i^*(x_i^*, y^*)$, the condition

$$\left(a\left(\eta+\frac{1-\eta}{1+ky^*}\right)-d-bx_i^*-\frac{cy^*}{1+x_i^*}\right)=0$$

implies

$$H_1(x_i^*, y^*)=\frac{x_i^*}{x_i^*+u}\left(-bx_i^*+\frac{cx_i^*y^*}{(1+x_i^*)^2}\right),$$

aligning their stability with Theorem 2.3. Since the stability of E_1 and E_i^* is unchanged, only the boundary equilibria E_0 and E_2 require further analysis.

For $E_0(0,0)$, it is straightforward to ascertain that the two eigenvalues of $J(E_0)$ are $\lambda_1=0$ and $\lambda_2=1>0$, indicating that E_0 is degenerate. Expanding system (1.9) around the origin up to the third order gives the following form:

$$\begin{cases}\dfrac{dx}{dt}=\dfrac{a-d}{u}x^2-\dfrac{bu+a-d}{u^2}x^3+\dfrac{a\eta k-ak-c}{u}x^2y+O(|x,y|^3),\\[2ex] \dfrac{dy}{dt}=y-ey^2.\end{cases}\tag{4.2}$$

According to Theorem 7.1 in Zhang [42], we can know that $m=2, a_m=\frac{a-d}{u}>0$, so $E_0(0,0)$ is a repelling saddle-node.

For $E_2(0,\frac{1}{e})$, it is straightforward to ascertain that the two eigenvalues of $J(E_2)$ are $\lambda_1=0$ and $\lambda_2=-1<0$, indicating that E_2 is degenerate. Expanding system (1.9) around the origin up to the fourth order. We make the following transformation:

$$X=x,\ Y=y-\frac{1}{e},\ d\tau=-dt.$$

The resulting system (1.9) is:

$$\begin{cases}\dfrac{dX}{d\tau}=a_{20}X^2+a_{30}X^3+a_{21}X^2Y+a_{40}X^4+a_{31}X^3Y+O(|X,Y|^4),\\[2ex] \dfrac{dY}{d\tau}=Y+eY^2,\end{cases}\tag{4.3}$$

where

$$\begin{aligned}a_{20}&=-\frac{ae\eta k+ae^2-de^2-dek-ce-ck}{eu(k+e)},\ a_{21}=-\frac{ae^2k\eta-ae^2k-ce^2-2cek-ck^2}{u(k+e)^2},\\ a_{30}&=\frac{ae\eta k+bue^2-beuk+ae^2-cue-cuk-de^2-dek-ce-ck}{eu^2(k+e)},\\ a_{40}&=-\frac{a_{30}-ceu^2-cku^2}{eu^3(k+e)},\ a_{31}=\frac{a_{21}-2e^2u-2ceku-cku^2}{u^2(k+e)^2}.\end{aligned}$$

Utilizing the central manifold theorem, the constrained system limited to the central manifold is expressed as follows:

$$\frac{dX}{d\tau}=a_{20}X^2+a_{30}X^3+a_{40}X^4+O(X^4).$$

We will now examine the subsequent cases.

Case 1. If $a_{20}\neq 0$, i.e., $c\neq c^{**}$, then $m=2,\ a_m=a_{20}=-\frac{ae\eta k+ae^2-de^2-dek-ce-ck}{eu(k+e)}$.

If $-a_{20} > 0$ (< 0), i.e., $c > (<, resp.)c^{**}$, E_2 is an attracting saddle-node with the parabolic sector situated on the right (left) half-plane, as per Theorem 7.1 in Zhang [42].

Case 2. If $-a_{20} = 0$ and $a_{30} \neq 0$, i.e., $c = c^{**}$ and $\eta \neq \eta^*$, then $m = 3, a_m = a_{30} = \frac{-eu((a-d-b)e+k(a\eta-b-d))}{eu^2(k+e)}$.
(i) If $a_{30} > 0$, i.e., $\eta < \eta^*$, E_2 is a degenerate stable node of codimension 2.
(ii) If $a_{30} < 0$, i.e., $\eta > \eta^*$, E_2 is a saddle of codimension 2.

Case 3. If $a_{20} = 0$ and $a_{30} = 0$, i.e., $c = c^{**}$ and $\eta = \eta^*$, then $m = 4$, $a_m = a_{40} = \frac{ceu^2+cku^2}{eu^3(k+e)} > 0$. E_2 is a codimension-3 attracting saddle-node, with the parabolic sector situated on the left half-plane.

The proofs for the positive equilibria $E_i^*(i = 1, 2, 3)$ and the boundary equilibrium E_1 are comparable to those of Theorems 2.2 and Theorem 2.3.

Theorem 4.1 has been fully proved. □

Table 2. Stability of equilibria in system (1.9) under different parameter conditions.

Equilibrium	Existence		Stability
$E_0(0,0)$	Always exists		repelling saddle-node
$E_1(\frac{a-d}{b}, 0)$	$a > d$		saddle
$E_2(0, \frac{1}{e})$	Always exists	$\eta > \eta^{**}$, $d < a < \frac{(k+e)(b+d)}{e}$	$c = c^{**}$, $\eta > \eta^*$, stable node
			$c = c^{**}$, $\eta < \eta^*$, saddle
			$c = c^{**}$, $\eta = \eta^*$, attracting saddle-node
			$c \neq c^{**}$, attracting saddle-node
$E_1^*(x_1^*, y^*)$	$0 < c \leq c^{**}$, $\eta > \eta^{**}$ and $d < a < \frac{(k+e)(b+d)}{e}$		stable node
	$c^{**} < c < c^*$, $\eta > \eta^*$, $b + d < a < \frac{d(k+e)}{e}$ and $k > \frac{eb}{d}$		
$E_2^*(x_2^*, y^*)$	$c^{**} < c < c^*$, $\eta > \eta^*$, $b + d < a < \frac{d(k+e)}{e}$ and $k > \frac{eb}{d}$		saddle
$E_3^*(x_3^*, y^*)$	$c = c^*$, $\eta > \eta^*$ and $b + d < a < \frac{(k+e)(b+d)}{e}$		attracting saddle-node

4.2. Bifurcation analysis

Theorem 4.2. *Transcritical bifurcation of system* (1.9) *occurs at* E_2 *when* $c = c^{**}$ *and* $\eta < \eta^*$. $c \equiv c^{**} = \frac{e(a\eta k+ea-de-dk)}{k+e}$ *is the value in this case.*

Theorem 4.3. *Pitchfork bifurcation of system* (1.9) *occurs at* E_2 *when* $c = c^{**}$ *and* $\eta = \eta^*$. *In this case,* $c^{**} = \frac{e(ak\eta+ea-ed-dk)}{k+e}$, $\eta^* = \frac{-(ae-be-bk-de-dk)}{ka}$.

Theorem 4.4. *Saddle-node bifurcation of system* (1.9) *occurs at* E_3^* *when* $c = c^*$ *and* $\eta > \eta^*$. *The bifurcation parameter* c *is defined as follows:*

$$c \equiv c^* = \frac{e(a\eta k + be + bk + ea - de - dk)^2}{4b(k+e)^2}.$$

4.3. Global structure

We can similarly apply the methods for analyzing global dynamical characteristics from Section 2.5 to system (1.9). We can represent the singularities at infinity and their stability qualities for system (1.9) by looking at the Poincaré transformation, as Figure 6 clearly illustrates. Similarly, Figure 7-Figure 10 vividly illustrate the global phase portraits of system (1.9) in the first quadrant.

5. Numerical simulations

5.1. Sensitivity analysis

In the parameter optimization and mechanistic interpretation of ecological dynamic models, minor perturbations in system parameters often propagate through nonlinear mechanisms to produce complex ecological responses. Sensitivity analysis, as a core diagnostic technique in modeling, quantifies the intensity of population dynamics responses to parameter perturbations, enabling systematic identification of key determinants controlling population behaviors. This study focuses on the amensalism system (1.9) and employs a dual-metric evaluation framework comprising semi-relative sensitivity $S_{i,j}$ and logarithmic sensitivity $\hat{S}_{i,j}$ analyses [29–31]:

$$S_{i,j} = q_j \frac{\partial u_i}{\partial q_j}, \ \hat{S}_{i,j} = \frac{q_j}{u_i} \frac{\partial u_i}{\partial q_j},$$

where u_i is the response variable (x or y), q_j is a system parameter $(a, b, c, d, e, k, \eta, u)$ and $\frac{\partial u_i}{\partial q_j}$ is the partial derivative of the response variable u_i with respect to the parameter q_j. Using MATLAB numerical simulations, we obtained the semi-relative sensitivity and logarithmic sensitivity of the system parameters to the populations x and y, as shown in Figure 17.

As illustrated in Figure 17(a) and (c), the dynamical behavior of population x exhibits significant positive sensitivity to parameter a (intrinsic growth rate of population x), η (saturated fear parameter), and e (intraspecific competition coefficient of population y). Conversely, parameters k (fear level), d (mortality rate of population x), b (intraspecific competition coefficient of population x), c (the direct impact of population y on population), and u (Allee effect parameter) demonstrate negative regulatory impacts on population x. Notably, the peak positive sensitivity values significantly exceed the magnitudes of negative attenuation effects, indicating that sufficiently high values of these positive parameters can ensure the long-term persistence of population x. Specifically, the regulatory efficacy of η surpasses both k and u, while the suppressive impact of u is weaker than that of k, suggesting that the saturated fear effect exerts a more pronounced influence on population x compared to the Allee effect. Temporal analysis reveals that all sensitivity curves converge to stable equilibria when $t \geq 10$, signifying the completion of transient dynamics and establishment of steady-state population regulation. Meanwhile, sensitivity analysis for population y (Figure 17(b) and (d)) identifies parameter e (intraspecific competition coefficient of population y) as its sole significant negative regulator, consistent with the classical theoretical predictions of amensalistic interactions in asymmetric competition frameworks.

To more intuitively observe the influence of the saturation fear function on population density, we analyzed the relationship between fear level k, saturation fear parameter η, and the equilibrium density of species x under coexistence conditions, along with their corresponding contour plots. Our findings reveal that when the saturation fear parameter η exceeds a certain threshold, the first species does not face extinction even as the fear level k approaches infinity. To verify the survival of the first species under high fear levels, we examined the range $\eta \in (0.6, 1)$ and $k \in (0, 2000)$, as shown in Figure 18 (c). The results clearly demonstrate that the first species can persist even under extreme fear conditions.

Ecologically, as the fear level k increases, the fear effect exerted by the second species on the first does not grow linearly but instead exhibits saturation. This means that even at high fear levels, the first species can sustain a certain degree of reproduction and survival. This phenomenon may be attributed to adaptive mechanisms in the first species, such as behavioral

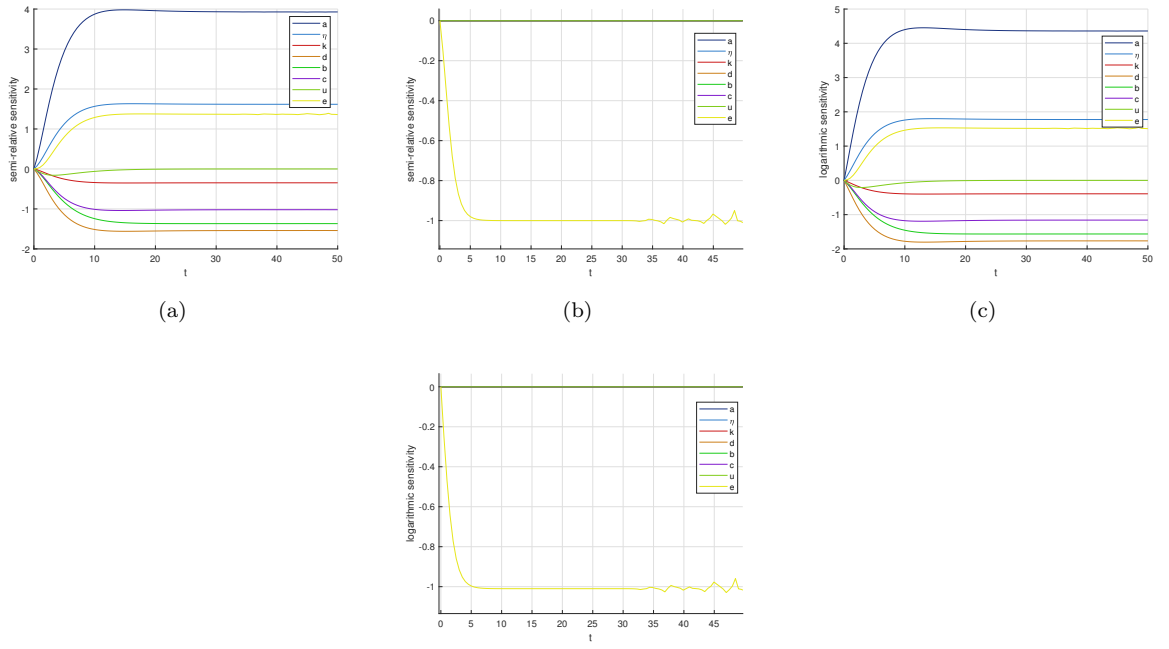

(a) (b) (c)

(d)

Figure 17. Fix parameters $(a, b, c, d, e, k, \eta, u) = (3, 1, 1.25, 1, 1, 1, 0.7, 1)$. Parameter sensitivity analysis of population dynamics: (a)(b) semi-relative sensitivity, (c)(d) logarithmic sensitivity.

modifications (e.g., avoiding habitats densely populated by the second species or enhancing reproductive output) to counteract the adverse effects of fear-driven stress.

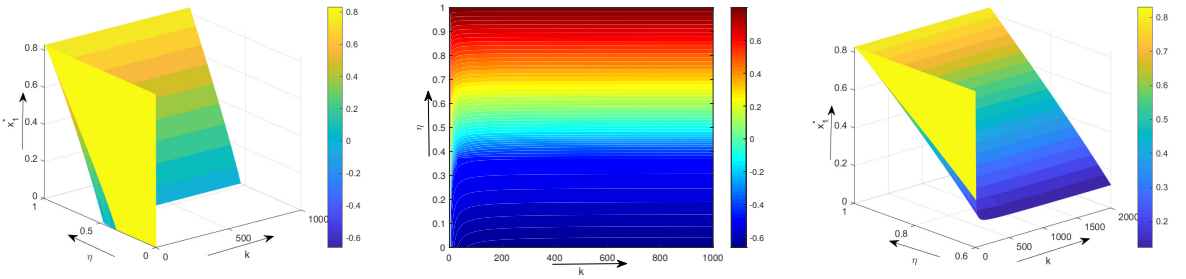

(a) (b) (c)

Figure 18. (a) Fix parameters $(a, b, c, d, e, u) = (3, 1, 1.25, 1, 1, 1)$, (a) 3D plot of (k, η, x_1^*): The effects of fear level k and saturation parameter η on x_1^*, (b) contour plot corresponding to Figure (a), (c) 3D plot of (k, η, x_1^*) with $k \in (0, 2000)$ and $\eta \in (0.6, 1)$.

5.2. Effect of η on the dynamics of the system

As indicated in Table 1, we note that when $0 < c \leq c^{**}(\eta > \eta^{**})$ or $c^{**} < c < c^*$ and $\eta > \eta^*$, system (1.7) there must exist a stable positive equilibrium E_1^*. Therefore, we conclude that when $0 < c \leq c^{**}$ or $c^{**} < c < c^*$, η falls in the interval $(\eta^{**}, 1)$ or $(\eta^*, 1)$, as the saturated fear parameter η increases, it will only rise the density of the first population, and has no influence on the extinction or survival of the first population. However, when η falls outside the interval

$(\eta^{**}, 1)$ or $(\eta^*, 1)$, an increase in the saturated fear parameter η will slow down the extinction process of the first species population. We next confirm this using numerical simulation using the time-course graphs of solutions.

Example 5.1. For $0 < c < c^{**}$, the case where $(a, b, d, e, k) = (7, 1, 5, 1, \frac{1}{2})$ is examined. As shown in Figure 19, when $\eta > \eta^{**} = \frac{1}{7}$, as the saturated fear parameter η increases, the density of the first species rises without affecting the species' ultimate extinction or survival; when $\eta < \eta^{**} = \frac{1}{7}$, an increase in the saturated fear parameter η will slow down the extinction process of the first species population.

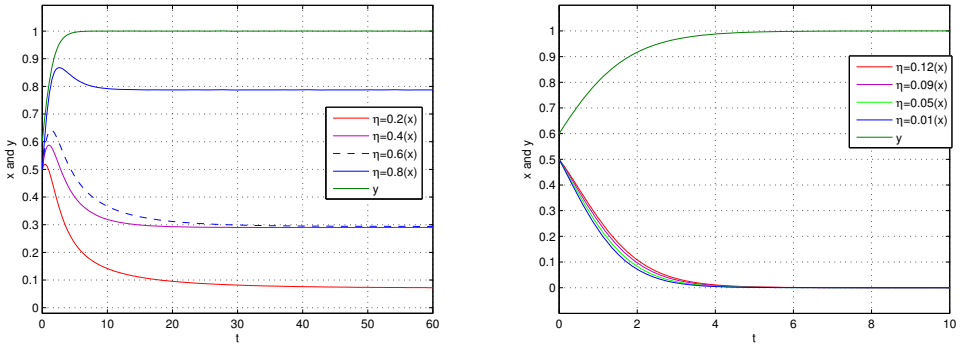

(a) (b)

Figure 19. In (a), both species coexist when $\eta > \eta^{**}$; In (b), the first species becomes extinct while the second endures when $\eta < \eta^{**}$.

Example 5.2. For $c^{**} < c < c^*$, we consider the situation when $(a, b, d, e, k) = (7, 1, 5, 1, \frac{1}{2})$, Based on the time series plot (Figure 20), we have the following findings. When $\eta > \eta^* = \frac{4}{7}$, as the saturated fear parameter η increases, the density of the first species rises without affecting the species' ultimate extinction or survival. When $\eta < \eta^* = \frac{4}{7}$, an increase in the saturated fear parameter η will slow down the extinction process of the first species population.

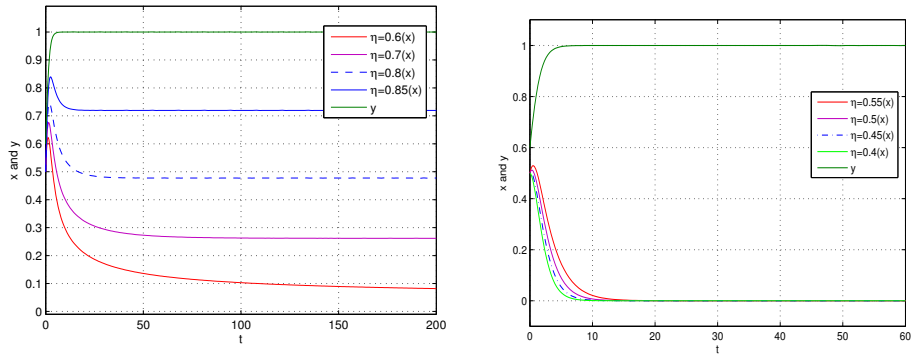

(a) (b)

Figure 20. In (a), both species cohabit when $\eta > \eta^*$; In (b), the first species becomes extinct while the second species endures when $\eta < \eta^*$.

Remark 5.1. From Example 5.1 to Example 5.2, we observe that under specific conditions, when the saturated fear parameter η surpasses a certain threshold, increasing the value of this parameter will lead to a rise in the density of the first species population, without influencing its survival or causing extinction, indicating that the saturated fear effect mitigates the negative impact of fear, allowing the species to thrive. Conversely, if the saturated fear parameter η drops below this threshold, an increase in the saturated fear parameter η will slow down the extinction process of the first species population.

5.3. Globally stability

We will demonstrate the global stability of the equilibria in Theorems 2.9 and 2.10 through numerical simulations in Examples 5.3 and 5.4.

Example 5.3. Theorem 2.9 states that E_2 is globally asymptotically stable for $c > c^{**}$ and $\eta \leq \eta^*$. We consider the situation when $(a, b, c, d, e, k, \eta) = (7, 1, \frac{1}{3}, 5, 1, \frac{1}{2}, \frac{1}{5})$. Numerical simulation results (Figure 21) confirm that $E_2(0, 1)$ is globally asymptotically stable.

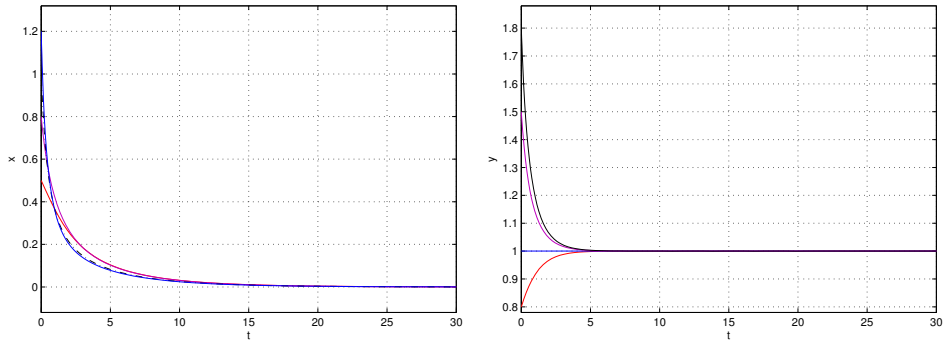

Figure 21. Taking the initial values as $(0.5, 0.8)$, $(0.8, 1.0)$, $(1.0, 1.5)$ and $(1.2, 1.8)$, respectively.

Example 5.4. Theorem 2.10 states that E_1^* is globally asymptotically stable for $0 < c < c^{**}$. We examine the situation when $(a, b, c, d, e, k, \eta) = (7, 1, \frac{43}{36}, 5, 1, \frac{1}{2}, \frac{5}{7})$. Numerical simulation results (Figure 22) confirm that $E_1^*(0.574882521, 1)$ is globally asymptotically stable.

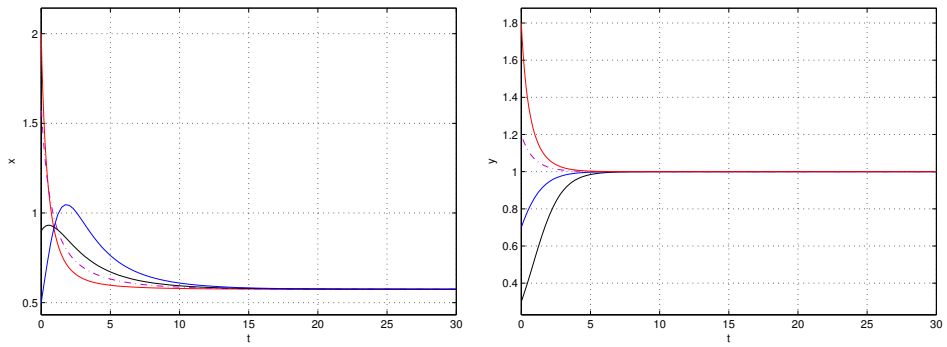

Figure 22. Taking the initial values as $(2, 1.8)$, $(1.6, 1.2)$, $(0.9, 0.7)$ and $(0.5, 0.3)$, respectively.

5.4. Bifurcations

Figures 23(a)-(b) illustrate bifurcation diagrams using c as the bifurcation parameter, supporting Section 2.3's theory on transcritical, saddle-node and pitchfork bifurcation within certain parameters [8]. Figure 23(c) illustrates the bifurcation diagram with η as the bifurcation parameter, allowing for the following observations. By adjusting other factors, η is relatively small. There is only one stable boundary equilibrium E_2, signifying the extinction of the first species while the second species endures. As η incrementally rises, the global stability of the boundary equilibrium E_2 shifts to bistability between the boundary equilibrium and the positive equilibrium, indicating that an elevation in the saturated fear parameter η can facilitate the stable coexistence of both species. This transition is induced by saddle-node bifurcation. As η attains a certain value, the positive equilibrium E_2^* converges with the boundary equilibrium E_2, transitioning into the second quadrant and altering its stability. The positive equilibrium E_1^* becomes globally stable, indicating that the coexistence of both species will be maintained. This process is governed by transcritical bifurcation.

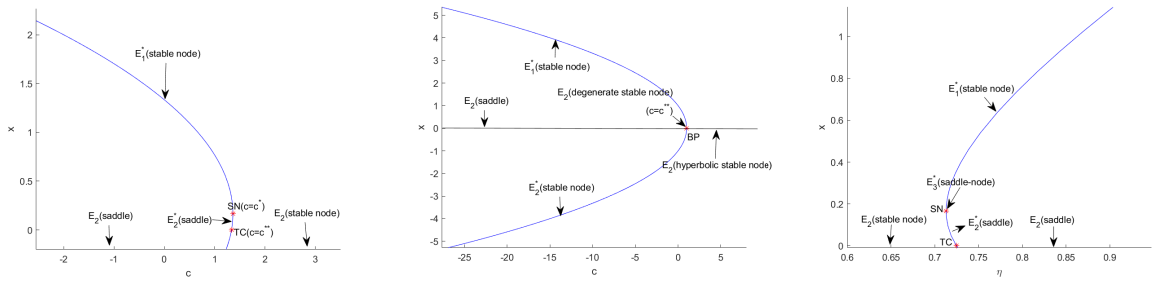

(a) (b) (c)

Figure 23. Parameters:$a = 7,\ b = e = 1,\ d = 5,\ k = \frac{1}{2}$. In (a), with $\eta = \frac{5}{7}$, saddle-node bifurcation occurs at $c = c^* = \frac{49}{36}$ whereas transcritical bifurcation occurs at $c = c^{**} = \frac{4}{3}$; In (b), with $\eta = \frac{4}{7}$, pitchfork bifurcation is observed at $c = c^{**} = 1$; In(c), with $c = 1.358$, we observed pitchfork bifurcation and saddle-node bifurcation.

5.5. The effect of Allee effect

In this sction, we will employ numerical simulations of the amensalism model, both incorporating and excluding the Allee effect, to illustrate how the Allee effect in the first species affects the local stability of areas $G_i (i = 1, 2, 3, 4)$.

Remark 5.2. The Allee effect will modify the equilibrium type, although it will not influence the overall dynamics in the first quadrant. As shown in Figures 24(a)-(d), the Allee effect on the first species does not alter the ultimate stable steady-state solution of the two species. With the Allee effect, the system (1.9) prolongs the time it takes for the system to rearch the steady-state compared to the system without it. As the value of u escalates, the first species in system (1.9) will need an extended duration to attain its stable steady-state solution. Nevertheless, this does not influence the time required for the second species to achieve its respective stable equilibrium.

6. Conclusions

We introduce the saturated fear effect into an amensalism model with Holling-II functional response and Allee effect, revealing its impact on species coexistence and extinction thresholds.

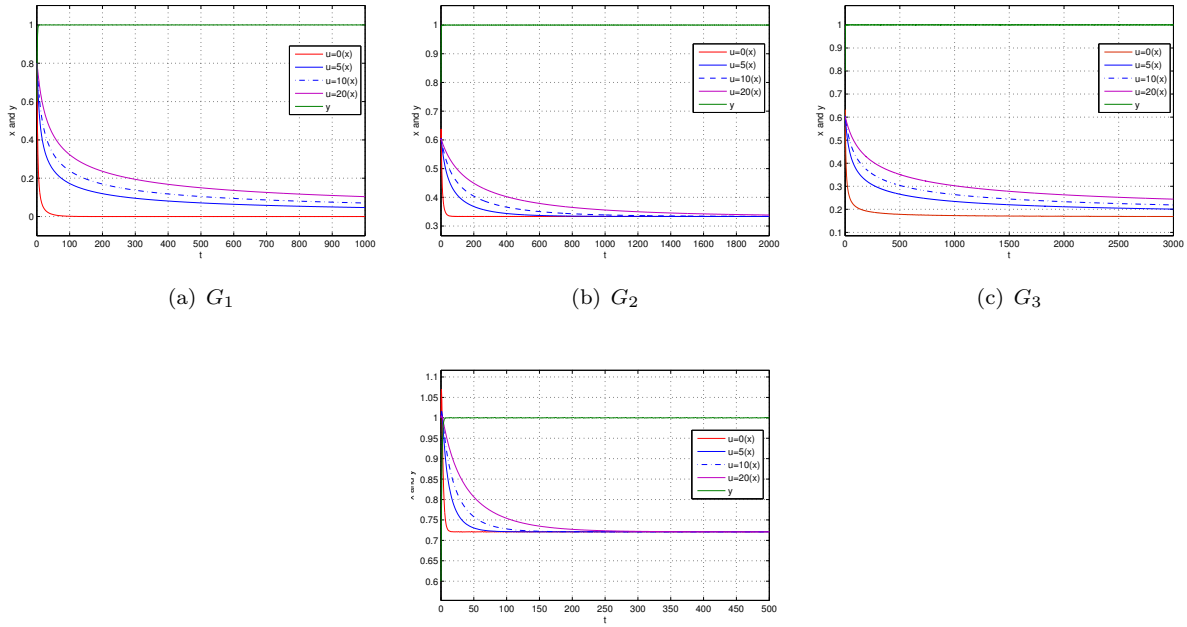

(a) G_1 (b) G_2 (c) G_3

(d) G_4

Figure 24. The impact of weak Allee effect on the first species in $G_i(i = 1, 2, 3, 4)$

We can conclude from theoretical study and numerical simulations:

- Introduction of Saturated Fear Effect: This study is the first to introduce the saturated fear effect into a two-species amensalism system. Through theoretical analysis and numerical simulations, we have discovered that when the saturated fear parameter exceeds a certain threshold, even extremely high fear levels will not lead to the extinction of the first species. This finding reveals the saturation characteristics of the fear effect under high intensity, indicating that the saturated fear effect can help species maintain population stability and avoid extinction under high fear pressure. In addition, in an appropriate parameter range, the saturation fear effect can induce bistability in the system (1.7), meaning the system simultaneously exhibits a stable coexistence state (E_1^*) and an extinction state of species x (E_2). To more accurately characterize the dynamical behavior of this bistability in real-world environments, we introduce stochastic perturbations to establish the stochastic system (3.1). Numerical simulations reveal that species x exhibits significant sensitivity to random disturbances: under moderate noise intensity, the stochastic system transitions from the coexistence state E_1^* to the extinction state E_2; when the noise intensity further increases beyond a critical threshold, the stochastic system evolves into a state of joint extinction for both species. Using the stochastic sensitivity function technique, we estimated the critical noise threshold for the transition from E_1^* to E_2 by constructing confidence ellipses, which aligns with the phenomenon of "sudden extinction" observed in real ecological systems.
- Introduction of Allee Effect: This study incorporates the weak Allee effect into the first species and finds that while it does not alter the final steady-state solution of the system, it significantly prolongs the time required for the system to reach equilibrium. Particularly, when the saturated fear parameter falls below the threshold, the Allee effect can slow down

the extinction process of the first species. From an ecological perspective, the Allee effect acts as a buffer when species are on the brink of extinction, delaying the extinction process.

- Bifurcation Behavior: When η is relatively small, the system possesses only a single stable boundary equilibrium E_2, indicating that under low saturated fear levels, the first species cannot survive in the ecosystem. As η increases to a critical threshold, the boundary equilibrium E_2 loses its global stability, leading to the emergence of bistability. A saddle-node bifurcation occurs, resulting in the coexistence of the boundary equilibrium E_2 and a stable positive equilibrium E_1^*. This implies that when the saturated fear level increases to a certain extent, the first species has the potential to persist in the ecosystem. When η reaches a specific threshold, the positive equilibrium E_2^* merges with the boundary equilibrium E_2 and shifts into the second quadrant, triggering a transcritical bifurcation. Consequently, the positive equilibrium E_1^* becomes globally stable, signifying that both species can achieve long-term coexistence. Research findings suggest that the saturated fear effect can facilitate species coexistence rather than merely suppressing the survival of the first species. Specifically, when η is sufficiently large, even under high fear levels, the first species can still maintain a stable population density. This phenomenon generally manifests as behavioral adaptations of the first species in high-fear environments, such as reducing encounters with the second species or enhancing reproductive capacity, thereby sustaining its survival and contributing to the formation of a stable ecological structure.

Compared to the findings of Chong [7], our system (1.7) exhibits a significantly increased number of equilibria and demonstrates more complex and diverse dynamic behaviors. At these equilibria, we have observed potential bifurcation phenomena: the system may undergo transcritical bifurcation and saddle-node bifurcation at E_2, while saddle-node bifurcation may occur at E_3^*. In contrast to Zhu's research [46], our consideration of the saturated fear effect better aligns with ecological reality. Zhu [46] demonstrated that increasing fear levels would reduce the population density of the first species without affecting its extinction or persistence; however, when fear exceeded a certain threshold, further increases would accelerate the first species' extinction. In contrast, our study demonstrates through theoretical analysis and numerical simulations of parameter sensitivity that: when the saturation fear parameter exceeds a specific threshold, even extremely high fear levels no longer lead to the first species' extinction; yet when the saturation fear parameter falls below this threshold, excessive fear levels can still cause extinction, though the presence of the weak Allee effect significantly slows this extinction process. Furthermore, our incorporation of environmental noise into the amensalism system provides more realistic simulations. This result not only fills the gap in understanding the saturated fear effect in amensalism systems but also provides new perspectives and theoretical support for understanding how species can self-regulate under amensal stress. The introduction of environmental stochasticity enables better predictions of population dynamics in natural systems subject to random perturbations.

In field studies, how should we measure the saturated fear parameter η? Taking Akimoto's [1] experiment as an example, we first determine the baseline reproduction rate, which is the daily average egg production of sp.O under isolated culture conditions, serving as the maximum reference value for reproductive capacity. Subsequently, through multi-species co-culture experiments, we measure the actual egg production of sp.O when coexisting with other aphid species, i.e., the mixed-culture reproduction rate. The calculation of the fear saturation parameter (η) can employ two mutually verifying methods: First, the fear saturation parameter was calculated by taking the ratio of the mixed-culture reproduction rate to the baseline

reproduction rate (η = Rmixed/Rbaseline), which directly quantifies the degree of reproductive inhibition; Second, by establishing a gall density gradient experiment, when the gall density approaches extremely high values, observe the proportion at which the reproduction rate of sp.O stabilizes—this asymptotic value serves as the direct measurement result of η. The consistency between the results obtained by these two methods (e.g., $\eta \approx 0.6$) not only verifies the reliability of the measurements but also reveals the ecological adaptation characteristics of sp.O, which can maintain approximately 60% of its baseline reproductive capacity even under extreme fear pressure.

In nature, the fear effect induced by the second species on the first species may not only result in a decrease in birth rates but also contribute to an increase in mortality rates [7]. Therefore, future research could explore models where both the birth and mortality rates of the first species are influenced by a saturated fear effect. Moreover, the birth rates of many populations are not simply linear growth; they are affected by environmental factors, resource availability, and population density. For instance, when population density is high, intensified competition may lead to a decrease in birth rates, whereas, under abundant resource conditions, birth rates may increase sharply [4, 22]. Therefore, incorporating nonlinear birth rates into the model of the second species is essential. These issues will be reserved for further exploration in our subsequent research.

References

[1] S. Akimoto, *Coexistence and weak amensalism of congeneric gall-forming aphids on the Japanese elm*, Population Ecology, 1995, 37(1), 81–89.

[2] A. R. S. Abd Alhadi and R. K. Naji, *The contribution of amensalism and parasitism in the three-species ecological system's dynamic*, Communications in Mathematical Biology and Neuroscience, 2024, 2024, 33–45.

[3] I. Bashkirtseva and L. Ryashko, *Sensitivity analysis of stochastic attractors and noise-induced transitions for population model with Allee effect*, Chaos: An Interdisciplinary Journal of Nonlinear Science, 2011, 21, 047514.

[4] B. Chen, *Dynamic behaviors of a non-selective harvesting Lotka–Volterra amensalism model incorporating partial closure for the populations*, Advances in Difference Equations, 2018, 2018(1), 1–14.

[5] F. Chen, W. He and R. Han, *On discrete amensalism model of Lotka–Volterra*, Journal of Beihua University, 2015, 16, 141–144.

[6] F. Chen, M. Zhang and R. Han, *Existence of positive periodic solution of a discrete Lotka-Volterra amensalism model*, Journal of ShengYang University (Natural Science), 2015, 27(3), 251–254.

[7] Y. Chong, Y. Hou, S. Chen and F. Chen, *The influence of fear effect to the dynamic behaviors of Lotka-Volterra ammensalism model*, Engineering Letters, 2024, 32(6), 1233–1242.

[8] A. Dhooge, W. Govaerts and Y. A. Kuznetsov, *MATCONT: A MATLAB package for numerical bifurcation analysis of ODEs*, ACM Transactions on Mathematical Software (TOMS), 2003, 29(2), 141–164.

[9] Y. Dong, D. Wu, C. Shen and L. Ye, *Influence of fear effect and predator-taxis sensitivity on dynamical behavior of a predator–prey model*, Zeitschrift für Aangewandte Mathematik und Physik, 2022, 73(1), 1–17.

[10] X. Guan and F. Chen, *Dynamical analysis of a two species amensalism model with Beddington–DeAngelis functional response and Allee effect on the second species*, Nonlinear Analysis: Real World Applications, 2019, 48, 71–93.

[11] X. Guan, Y. Liu and X. Xie, *Stability analysis of a Lotka-Volterra type predator-prey system with Allee effect on the predator species*, Communications in Mathematical Biology and Neuroscience, 2018, 2018(1), 9–23.

[12] X. Guo, L. Ding, Y. Hui and X. Song, *Dynamics of an amensalism system with strong Allee effect and nonlinear growth rate in deterministic and fluctuating environment*, Nonlinear Dynamics, 2024, 112(23), 21389–21408.

[13] M. E. Hibbing, C. Fuqua, M. R. Parsek and S. B. Peterson, *Bacterial competition: Surviving and thriving in the microbial jungle*, Nature Reviews Microbiology, 2010, 8(1), 15–25.

[14] Y. Kang and O. Udiani, *Dynamics of a single species evolutionary model with Allee effects*, Journal of Mathematical Analysis and Applications, 2014, 418(1), 492–515.

[15] R. Khasminskii, *Stochastic Stability of Differential Equations (Vol. 66)*, Springer Science & Business Media, 2011.

[16] C. Lei, *Dynamic behaviors of a stage structure amensalism system with a cover for the first species*, Advances in Difference Equations, 2018, 2018, 1–23.

[17] Q. Li, F. Chen, L. Chen and Z. Li, *Dynamical analysis of a discrete amensalism system with the Beddington-DeAngelis functional response and fear effect*, Journal of Applied Analysis & Computation, 2025, 15(4), 2089–2123.

[18] Q. Lin and X. Zhou, *On the existence of positive periodic solution of a amensalism model with Holling-II functional response*, Communications in Mathematical Biology and Neuroscience, 2017, 2017, 3. DOI: 10.28919/cmbn/2809.

[19] H. Liu, H. Yu, C. Dai, Z. Ma, Q. Wang and M. Zhao, *Dynamical analysis of an aquatic amensalism model with non-selective harvesting and Allee effect*, Mathematical Biosciences and Engineering, 2021, 18(6), 8857–8882.

[20] Y. Liu, L. Zhao, X. Huang and H. Deng, *Stability and bifurcation analysis of two-species amensalism model with Michaelis–Menten type harvesting and a cover for the first species*, Advances in Difference Equations, 2018, 2018, 1–19.

[21] D. Luo and Q. Wang, *Global dynamics of a Holling-II amensalism system with nonlinear growth rate and Allee effect on the first species*, International Journal of Bifurcation and Chaos, 2021, 31(03), 2150050.

[22] D. Luo and Q. Wang, *Global dynamics of a Beddington–DeAngelis amensalism system with weak Allee effect on the first species*, Applied Mathematics and Computation, 2021, 408, 126368.

[23] A. U. Mallik, *Allelopathy and competition in coniferous forests*, Environmental Forest Science, 1998, 54, 309–315.

[24] L. Perko, *Differential Equations and Dynamical Systems*, Springer-Verlag, NY, 2001.

[25] J. C. Polking, *Ordinary Differential Equations Using MATLAB*, Pearson Education India, 2009.

[26] S. Schreiber, *Allee effects, extinctions, and chaotic transients in simple population models*, Theoretical Population Biology, 2003, 64(2), 201–209.

[27] M. K. Singh, *Dynamical study and optimal harvesting of a two-species amensalism model incorporating nonlinear harvesting*, Applications & Applied Mathematics, 2023, 18(1), 19.

[28] G. Sun, *Qualitative analysis on two populations amensalism model*, Journal of Jiamusi University, 2003, 21(3), 283–286.

[29] J. P. Tripathi, S. S. Meghwani, M. Thakur and S. Abbas, *A modified Leslie–Gower predator-prey interaction model and parameter identifiability*, Communications in Nonlinear Science and Numerical Simulation, 2018, 54, 331–346.

[30] S. Wang, Z. Wang, C. Xu and G. Jiao, *Sensitivity analysis and stationary probability distributions of a stochastic two-prey one-predator model*, Applied Mathematics Letters, 2021, 116, 106996.

[31] S. Wang, Z. Xie, R. Zhong and Y. Wu, *Stochastic analysis of a predator–prey model with modified Leslie–Gower and Holling type II schemes*, Nonlinear Dynamics, 2020, 101, 1245–1262.

[32] Z. Wei, Y. Xia and T. Zhang, *Stability and bifurcation analysis of an amensalism model with weak Allee effect*, Qualitative Theory of Dynamical Systems, 2020, 19, 1–15.

[33] R. Wu, *Dynamic behaviors of a nonlinear amensalism model*, Advances in Difference Equations, 2018, 2018, 187. DOI: 10.1186/s13662-018-1624-9.

[34] R. Wu, *A two species amensalism model with non-monotonic functional response*, Communications in Mathematical Biology and Neuroscience, 2016, 2016, 19.

[35] R. Wu, L. Li and Q. Lin, *A Holling type commensal symbiosis model involving Allee effect*, Communications in Mathematical Biology and Neuroscience, 2018. DOI: 10.3934/cmb.2018.6.1.

[36] R. Wu, L. Zhao and Q. Lin, *Stability analysis of a two species amensalism model with Holling-II functional response and a cover for the first species*, Journal of Nonlinear Functional Analysis, 2016, 46, 1–15.

[37] X. Xi, J. N. Griffin and S. Sun, *Grasshoppers amensalistically suppress caterpillar performance and enhance plant biomass in an alpine meadow*, Oikos, 2013, 122(7), 1049–1057.

[38] X. Xie, F. Chen and M. He, *Dynamic behaviors of two species amensalism model with a cover for the first species*, Journal of Mathematics and Computer Science, 2016, 16(2), 395–401.

[39] W. Yin, Z. Li, F. Chen and M. He, *Modeling allee effect in the leslie-gower predator–prey system incorporating a prey refuge*, International Journal of Bifurcation and Chaos, 2022, 32(06), 2250086.

[40] J. Zhang, *Bifurcated periodic solutions in an amensalism system with strong generic delay kernel*, Mathematical Methods in the Applied Sciences, 2013, 36(1), 113–124.

[41] Z. Zhang, *Stability and bifurcation analysis for an amensalism system with delays*, Mathematica Numerica Sinica, 2008, 30(2), 213–224.

[42] Z. Zhang, T. Ding, W. Huang and Z. Dong, *Qualitative Theory of Differential Equations*, Science Press, Beijing, 1997.

[43] M. Zhao and Y. Du, *Stability and bifurcation analysis of an amensalism system with Allee effect*, Advances in Difference Equations, 2020, 2020, 1–13.

[44] M. Zhao, Y. Ma and Y. Du, *Global dynamics of an amensalism system with Michaelis-Menten type harvesting*, Electronic Research Archive, 2023, 31(2), 549–574.

[45] Q. Zhou and F. Chen, *Dynamical analysis of a discrete amensalism system with the Beddington–DeAngelis functional response and Allee effect for the unaffected species*, Qualitative Theory of Dynamical Systems, 2023, 22(1), 16.

[46] Q. Zhu, F. Chen, Z. Li and L. Chen, *Global dynamics of two-species amensalism model with Beddington–DeAngelis functional response and fear effect*, International Journal of Bifurcation and Chaos, 2024, 34(06), 245007.

Received February 2025; Accepted August 2025; Available online September 2025.